

CBE 60546

Heterogeneous Catalysis

William F. Schneider

Dept. of Chemical and Biomolecular Engineering

Dept. of Chemistry and Biochemistry

University of Notre Dame

wschneider@nd.edu

www.nd.edu/~wschnei1

Fall 2021

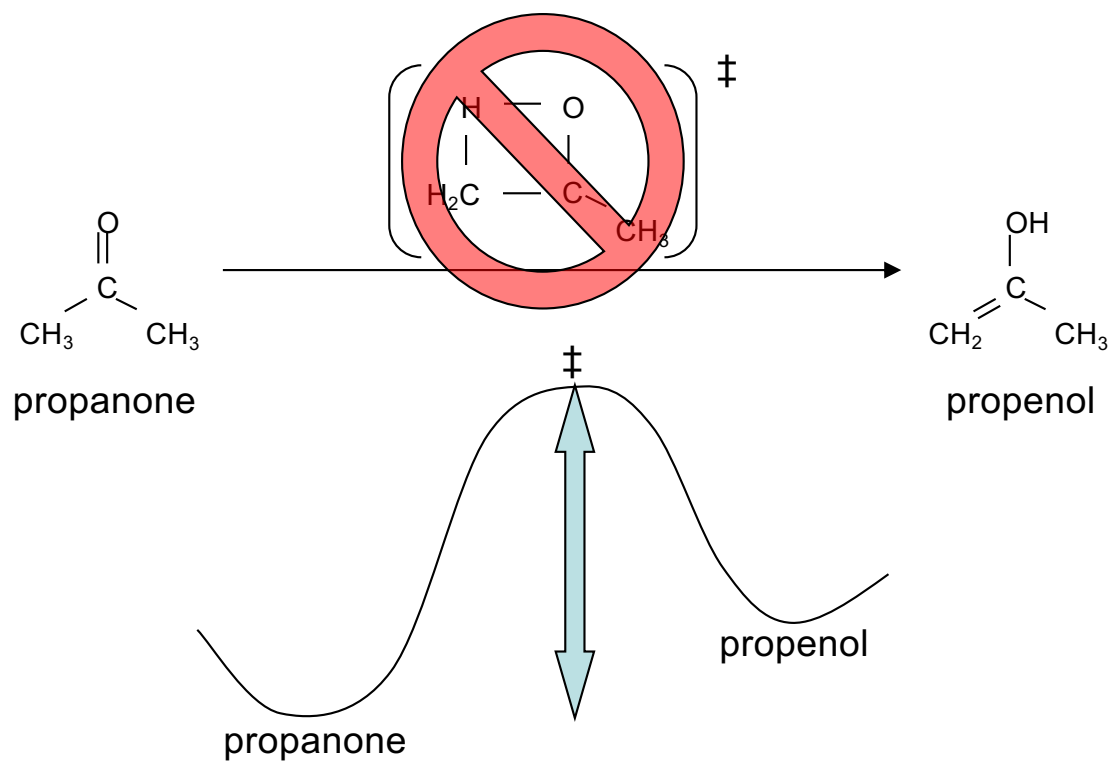


Definitions

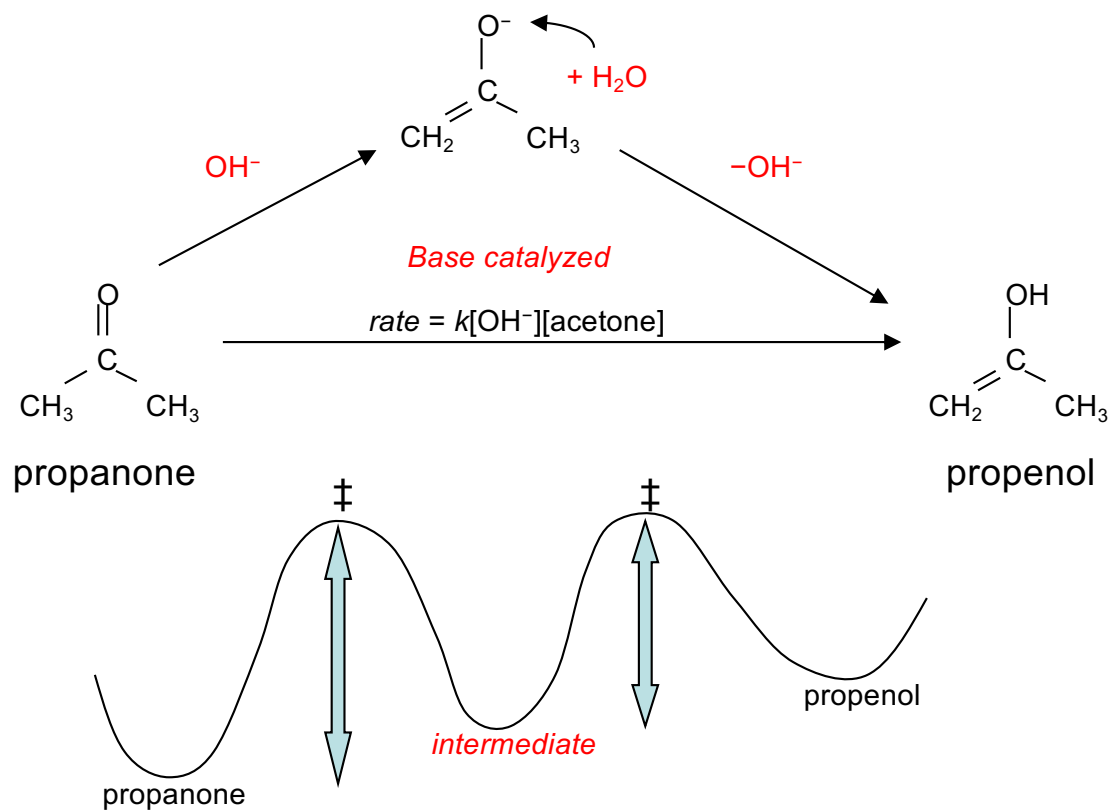
- **Catalyst** – a substance that accelerates the rate of a chemical reaction without itself being transformed or consumed by the reaction



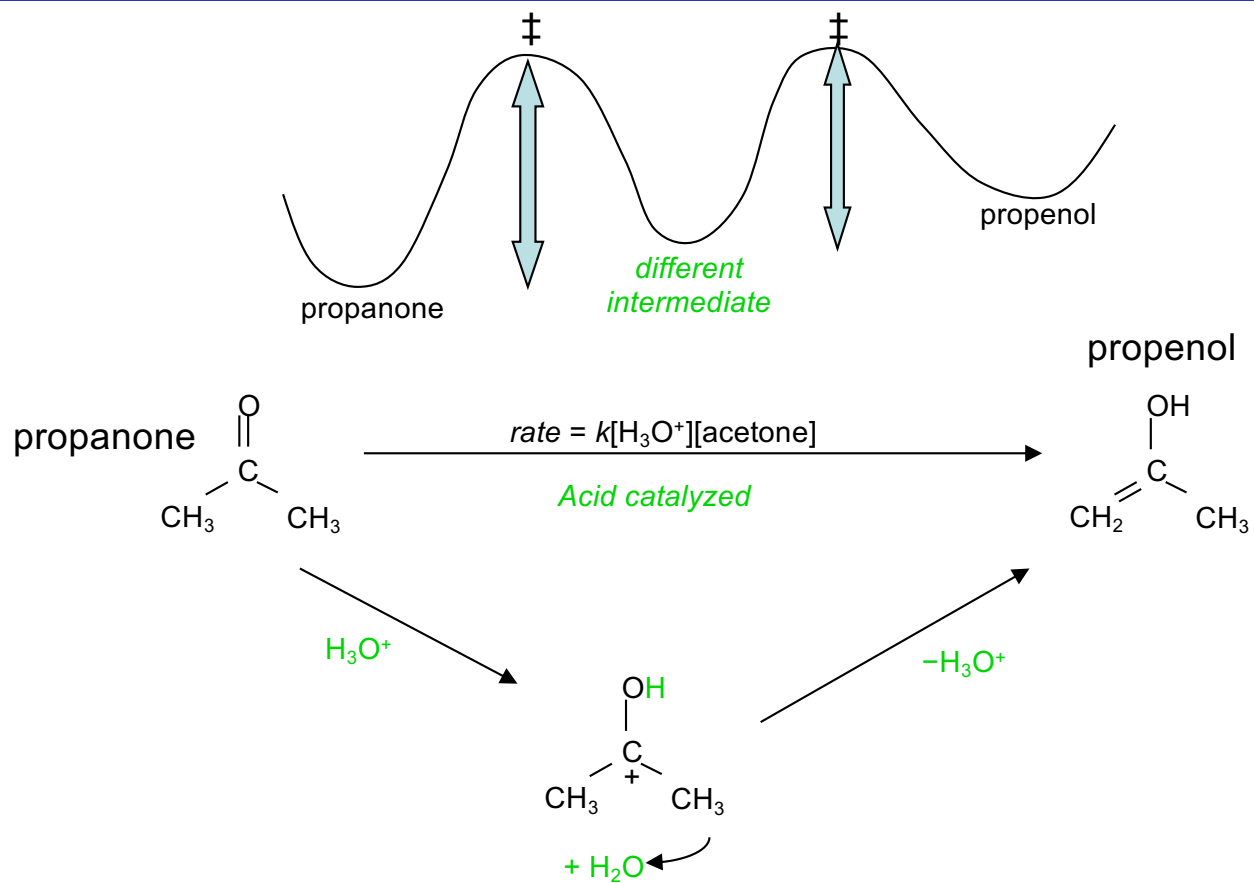
Catalysts Open Up New Reaction Pathways



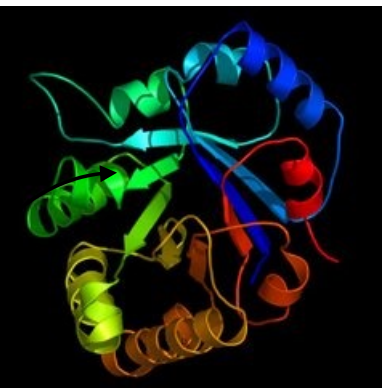
Catalysts Open Up New Reaction Pathways



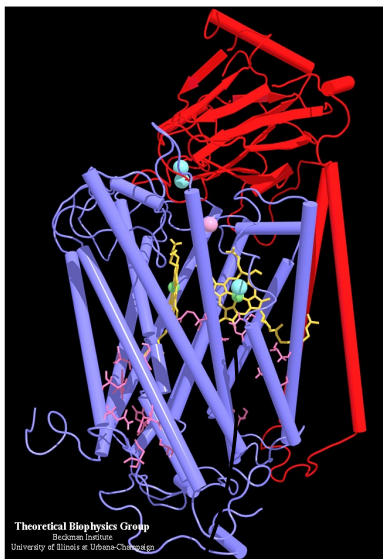
Catalysts Open Up New Reaction Pathways



Types of Catalysts - Enzymes



Triosephosphateisomerase
“TIM”



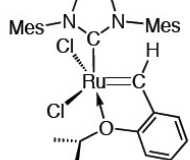
Cytochrome C Oxidase

Highly tailored “active sites”
Often contain metal atoms

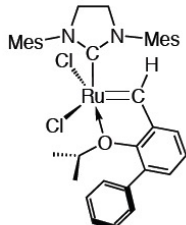
- The “Gold Standard” of catalysts
- Highly specific
- Highly selective
- Highly efficient
- Catalyze very difficult reactions
 - $\text{N}_2 \rightarrow \text{NH}_3$
 - $\text{CO}_2 + \text{H}_2\text{O} \rightarrow \text{C}_6\text{H}_{12}\text{O}_6$
- Works better in a cell than in a 100000 l reactor

Types of Catalysts – Organometallics

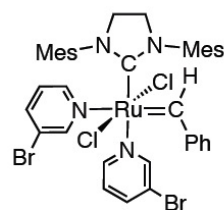
New Generation Catalysts



Grubbs-Hoveyda Catalyst

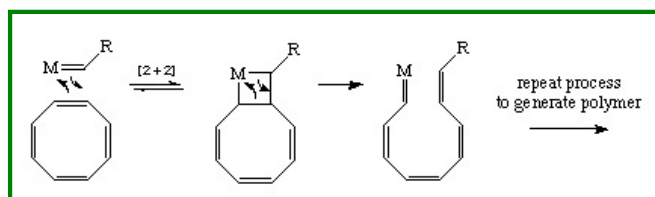


Blechert Catalyst

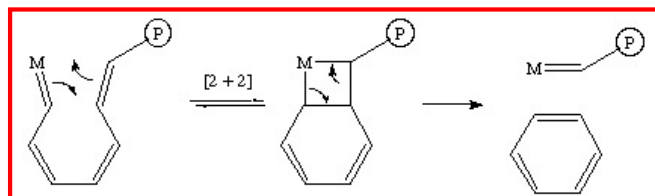


Grubbs "Fast Initiating Catalyst"

Polymerization:

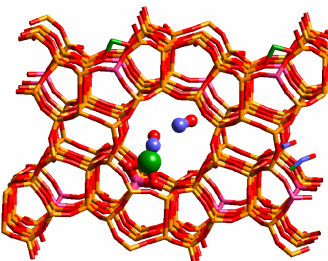
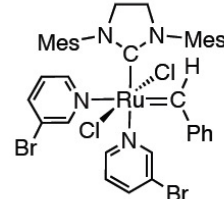
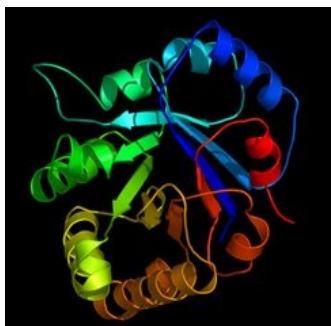


Termination:



- Perhaps closest man has come to mimicking nature's success
- 2005 Noble Prize in Chemistry
- Well-defined, metal-based active sites
- Selective, efficient manipulation of organic functional groups
- Various forms, especially for polymerization catalysis
- Difficult to generalize beyond organic transformations

Types of Catalysts – Homogeneous vs. Heterogeneous



Zeolite catalyst



Catalyst powders

Homogeneous catalysis

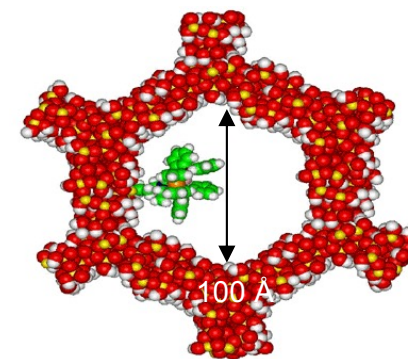
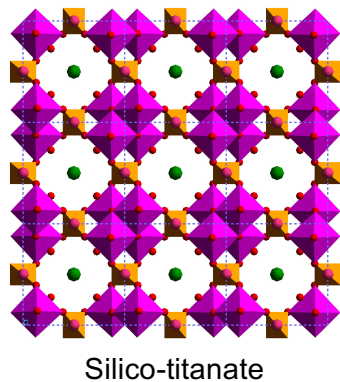
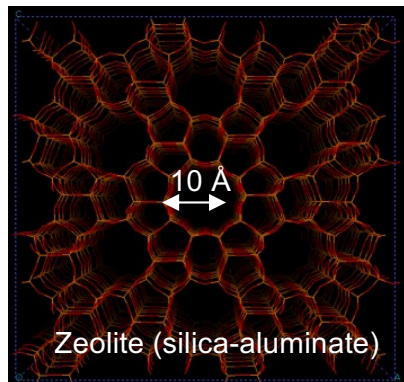
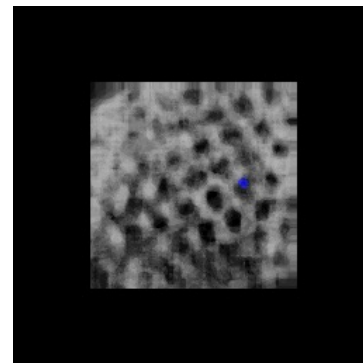
Single phase
(Typically liquid)
Low temperature
Separations are tricky

Heterogeneous catalysis

Multiphase
(Mostly solid-liquid and solid-gas)
High temperature
Design and optimization tricky

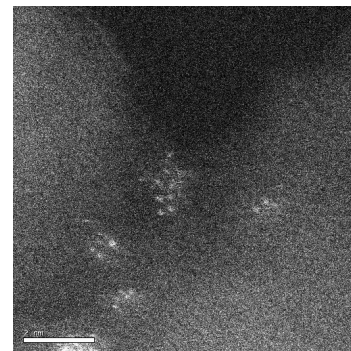
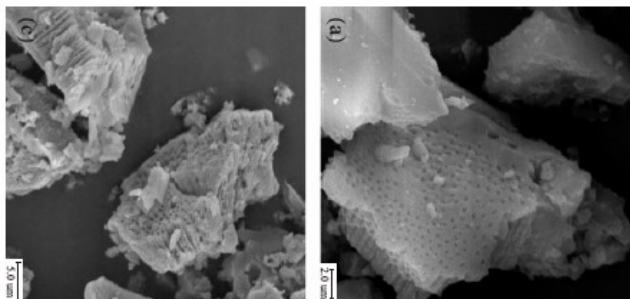
Types of Catalysts: Microporous Catalysts

- Regular crystalline structure
- Porous on the scale of molecular dimensions
 - 10 – 100 Å
 - Up to 1000's m²/g surface area
- Catalysis through
 - shape selection
 - acidity/basicity
 - incorporation of metal particles



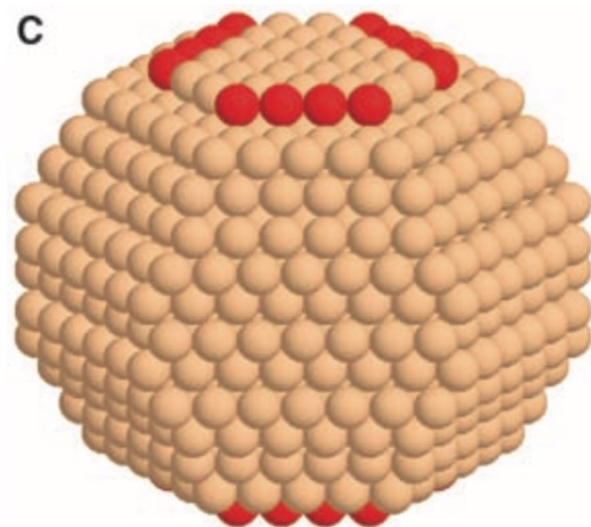
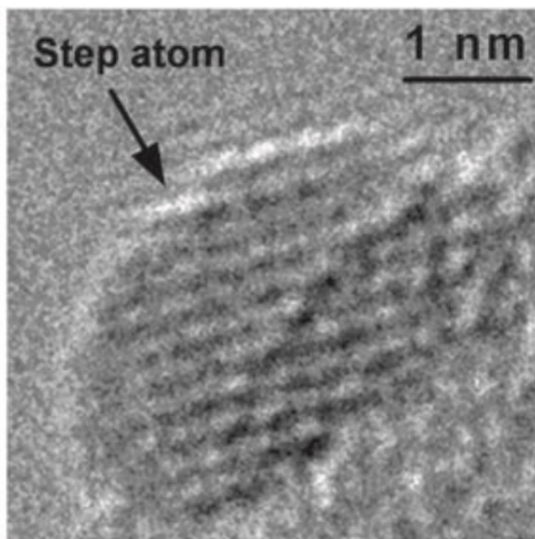
Types of Catalysts: Supported Metal Catalysts

- Amorphous, high surface area *supports*
 - Alumina, silica, activated carbon, ...
 - Up to 100's of m²/g of surface area
- Impregnated with catalytic *transition metals*
 - Pt, Pd, Ni, Fe, Ru, Cu, Ru, ...
- Typically pelletized or on monoliths
- Cheap, high stability, catalyze many types of reactions
- Most used, least well understood of all classes



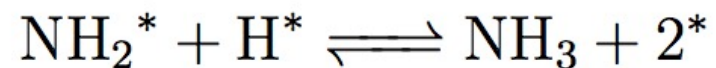
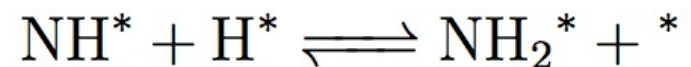
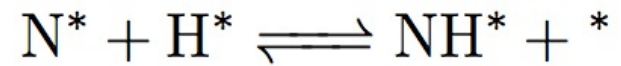
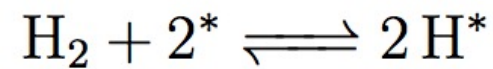
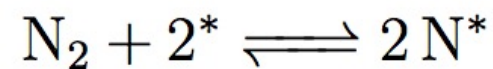
SEM micrographs of alumina and Pt/alumina

NH₃ Synthesis Catalysis



Honkala *et al. Science*, 307, 555, 2005.

Reaction is structure-sensitive
TOF_{steps} >> TOF_{terraces}



Important Energy-Related Catalysis

nature
catalysis

ARTICLES

<https://doi.org/10.1038/s41929-018-0045-1>

Overcoming ammonia synthesis scaling relations with plasma-enabled catalysis

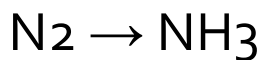
Prateek Mehta¹, Patrick Barbour¹, Francisco A. Herrera², Jongsik Kim¹, Paul Rumbach², David B. Go^{1,2}, Jason C. Hicks^{1*} and William F. Schneider^{1,2*}

Correlations between the energies of elementary steps limit the rates of thermally catalyzed reactions at surfaces. Here, we show how these limitations can be circumvented in ammonia synthesis by coupling catalysts to a nonthermal plasma. We postulate that plasma-induced vibrational excitations in N₂ decrease dissociation barriers without influencing subsequent reaction steps. We develop a density-functional-theory-based microkinetic model to incorporate this effect, and parameterize the model using N₂ vibrational excitations observed in a dielectric-barrier-discharge plasma. We predict plasma enhancement to be particularly great on metals that bind nitrogen too weakly to be active thermally. Ammonia synthesis rates observed in a dielectric-barrier-discharge plasma reactor are consistent with predicted enhancements and predicted changes in the optimal metal catalyst. The results provide guidance for optimizing catalysts for application with plasmas.

The rates of heterogeneous catalytic processes are governed by the adiabatic energies of reaction, the activation energies of activation, and the reaction pathways that connect these intermediate states. For a wide range of reactions on a variety of catalyst surfaces, it has been shown that the adsorption energies of various intermediates are correlated to one another by linear scaling relationships.^{1–3} Furthermore, activation energies and the related reaction rates are also often found to scale with the same linear relationships.^{4–7} When held constant, these relationships significantly reduce the number of independent parameters available for tuning catalyst performance, once placing a

A classic example of these two ammonia synthesis reaction. N₂ catalyst for this reaction should state for N₂ dissociation while sii NH₃ ($\chi = 0.1$ to 2) and the reactivity of the best known thermal catalysts of ammonia synthesis are correlated with each other on conventional metal catalysts, it is not possible to adjust these energies independently. As a consequence, optimization of these catalysts has been restricted along a volcano-type relation in a one-dimensional parameter space, and even the best identified materials, such as Pt and Ru, are only active at elevated temperatures (>700 K) and pressures (~100 atm). Finding ways to circumvent the scaling relations may provide a path towards enabling a more sustainable, low-temperature and -pressure ammonia synthesis process.^{8–10}

While the scaling relations for conventional metal catalysts remain elusive, one way of overcoming the above limitations is to assist nitrogen dissociation by applying an external stimulus. For instance, promotion of N₂ into less stable vibrational or electronically excited states may reduce the activation energy for N₂ dissociation without significantly impacting reaction steps. Thermal plasmas, generated by rapidly ionizing the source gas via an electric discharge, are rich sources of such vibrationally and electronically excited molecules, along with other reactive species such as radicals, ions and free electrons. Because these plasmas operate



type, plasma power, and so on) on performance.

In this article, we report an analysis that shows that ammonia synthesis scaling relations can be overcome through vibrational excitation of N₂ in a plasma-enabled catalytic process. Vibrational excitation is a natural starting point for the development of plasma catalysts. Vibrational excitation has significantly lower excitation energy thresholds compared with other forms of excitation (for example, electronic excitation, ionization or dissociation) and is thus a more effective excitation source for N₂ than for most plasmas.¹¹ Furthermore, the rates of dissociation of impinging gas molecules are known to increase when they are vibrationally excited.^{12–15}

We first build a microkinetic model that combines density functional theory (DFT)-calculated energies of ammonia synthesis and dissociation, and include activation energies of vibrational states extracted from the experimental characterization of a dielectric-barrier-discharge (DBD) plasma. The model shows that the optimal catalysts and active sites in plasma catalysis may differ from those in thermal catalysis. Moreover, the low-temperature and -pressure

¹Department of Chemical and Biomolecular Engineering, University of Notre Dame, Notre Dame, IN, USA. ²Department of Aerospace and Mechanical Engineering, University of Notre Dame, Notre Dame, IN, USA. *e-mail: jchicks3@nd.edu; ws Schneider@nd.edu

NATURE CATALYSIS | VOL.1 | APRIL 2018 | 269–275 | www.nature.com/natcat

© 2018 Macmillan Publishers Limited, part of Springer Nature. All rights reserved.



W. F. Schneider

Reductions

CHEM
CATALYST
CHEM
COMMUNICATIONS

ChemCatChem
Europe

DOI: 10.1002/cctc.201200839

Catalytic Hydrogenation of CO₂ to Formic Acid with Silica-Tethered Iridium Catalysts

Zheng Xu, Nicholas D. McNamara, Gregory T. Neumann, William F. Schneider, and Jason C. Hicks^{*†}

The combustion of fossil fuels as the primary source of chemical energy has led to the negative impact of CO₂ on our environment. To reduce the negative impact of CO₂ on our environment, we have developed a plasma-catalytic ammonia synthesis system to reduce the environmental impact of CO₂. With sufficient input of chemical energy, CO₂ can be converted to formic acid (FA) in the presence of a plasma fuel.^{1–4} Without a catalyst, these transformations are too slow to be of practical value and thus require sufficient chemical energy to drive the catalysts. A direct and promising approach to generating formic acid (FA) is the catalytic hydrogenation of CO₂ to formic acid (FA).^{5–7} Typical unsupported, homogeneous transition-metal catalysts capable of catalyzing this reaction include palladium, rhodium, and platinum.

There are few reports of heterogeneous catalysts for the reduction of CO₂ to FA.

In this study, a new silica-tethered iridium catalyst (Ir-PNS/SA-15) was synthesized for the hydrogenation of CO₂ to FA (Scheme 1). To the best of our knowledge, we report the first use of the tethered Ir catalyst for the selective hydrogenation of CO₂ to FA. In addition, the tethered Ir-supported ammonia-tethered Ru complex with a turnover frequency (TOF) of 1482 h⁻¹ for CO₂ hydrogenation to FA when PPh₃ was added under supercritical CO₂ conditions (80 °C, 18 MPa of total pressure).

In this study, a new silica-tethered iridium catalyst (Ir-PNS/SA-15) was synthesized and this species underwent metathesis with ICl, hydride in refluxing anhydrous ethanol to afford Ir-PNS/SA-15 (b) (Figure 1, see the Supporting Information for a detailed procedure). For comparison, an intermediate product, the tethered Ir-supported Ru complex with a turnover frequency (TOF) of 1482 h⁻¹ for CO₂ hydrogenation to FA when PPh₃ was added under supercritical CO₂ conditions (80 °C, 18 MPa of total pressure).

The tethered Ru hybrid materials were characterized by a battery of techniques including FTIR, UV-vis, thermogravimetric analysis (TGA), N₂ physisorption, inductively coupled plasma optical emission (ICP-OES) and X-ray photoelectron spectroscopy (XPS) (see the Supporting Information). The FTIR spectra of unsupported PNP^t and Ir-PNP^t showed the Schiff base (=CH-NR= double-bond absorption at 1639 cm⁻¹, as well as p phenyl ring vibrations at 3067, 1587, 1435, 743, and 694 cm⁻¹. Similar peaks also appeared in the FTIR spectra of

structure of the ligand was confirmed by ¹P NMR, ¹³C NMR, and ¹H NMR spectroscopy (Figures S1–S3, Supporting Information). The mesoporous silica support, SBA-15, was synthesized in a two-step procedure reported by N. P. Kovaleva et al.⁸ The resulting sample showed a type IV BET surface area of 950 m²/g and a Barrett-Joyner-Halenda (BJH) pore size of 6.2 nm (Table S1 and Figure S4, Supporting Information).

Ir-PNS/SA-15 (a) was synthesized by adding IrCl₃ onto SBA-15 to afford PNS/SA-15 (b) and this species underwent metathesis with ICl, hydride in refluxing anhydrous ethanol to afford Ir-PNS/SA-15 (b) (Figure 1, see the Supporting Information for a detailed procedure). For comparison, an intermediate product, the tethered Ir-supported Ru complex with a turnover frequency (TOF) of 1482 h⁻¹ for CO₂ hydrogenation to FA when PPh₃ was added under supercritical CO₂ conditions (80 °C, 18 MPa of total pressure).

The tethered Ru hybrid materials were characterized by a battery of techniques including FTIR, UV-vis, thermogravimetric analysis (TGA), N₂ physisorption, inductively coupled plasma optical emission (ICP-OES) and X-ray photoelectron spectroscopy (XPS) (see the Supporting Information). The FTIR spectra of unsupported PNP^t and Ir-PNP^t showed the Schiff base (=CH-NR= double-bond absorption at 1639 cm⁻¹, as well as p phenyl ring vibrations at 3067, 1587, 1435, 743, and 694 cm⁻¹. Similar peaks also appeared in the FTIR spectra of

RESEARCH

CATALYSIS

Dynamic multinuclear sites formed by mobilized copper ions in NO_x selective catalytic reduction

Christopher Paolucci,¹ Ishant Khurana,² Atish A. Parekh,² Siefi Li,¹ Arthur J. Shih,² Hui Li,¹ John R. Di Torio,² Jonatas D. Albaracin-Caballero,² Aleksey Yezerski,² Jeffrey T. Miller,² W. Nicholas Delgas,² Fabio H. Ribeiro,² William F. Schneider,^{1,*} Rajamani Gounder^{2,*}

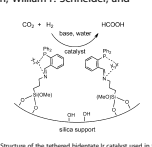
Copper ions exchanged into zeolites are active for the selective catalytic reduction (SCR) of nitrogen oxides (NO_x) with ammonia (NH₃), but the low-temperature rate dependence on copper (Cu) volumetric density is inconsistent with reaction at single sites. We combine steady-state and transient density measurements with X-ray absorption fine-structure (XAFS) and first-principles calculations to demonstrate that under reaction conditions, mobilized Cu ions can pass through zeolite windows and form ion pairs that participate in an oxygen (O₂)-mediated Cu²⁺-Cu⁰ redox step integral to SCR. Electrostatic tethering to framework aluminum centers limits the volume that each ion can explore and thus capacity to form an ion pair. The dynamic, reversible formation of multinuclear sites from mobilized single ions represents a distinct phenomenon that differs outside the conventional boundaries of a heterogeneous or homogeneous catalyst.

Single-site heterogeneous catalysts promise to combine the attractive features of homogeneous catalysts with the advantages of regiospecific and tunable heterogeneity that provide precise catalytic function, integrated into a thermally stable, porous, solid host that facilitates access of substrates to these sites and separation of products from the catalyst (Fig. 1). In the conventional definition a single-site catalyst cannot be active unless it is in equilibrium with Cu density at $\rho_{\text{Cu}} > 10^{-4}$ Å⁻³ (Fig. 1B), as would be expected for a reaction catalyzed by isolated Cu sites. Turnover rates, apparent reaction orders, and apparent activation energies (Table S1) are consistent with values reported for high-Cu density CuOx samples (Fig. 1B). By contrast, standard SCR rates vary quadratically with Cu density below $\rho_{\text{Cu}} < 1.3 \times 10^{-4}$ Å⁻³ (Fig. 1A). These rates are consistent with those reported for CuOx-CuO₂ samples with those reported for CuO₂-CuO₂ samples (Fig. 1B). Cu²⁺ ($\rho_{\text{Cu}} = 0.02$ (2)–(7); Si/Al = 6, Cu/Al < 0.05 (26)). We show that these two kinetic regimes are separated by distinct kinetic parameters, reflect different site-controlling density-stability steps, and prevalent reactive intermediates during steady-state NO_x SCR.

To probe the mechanistic origins of this change in kinetic regime, we used X-ray absorption fine-structure (XAFS) spectroscopy to quantify Cu oxidation state during steady-state standard SCR in operando. Figure 2 and Table S4 report the steady-state Cu⁰ fraction obtained by XANES fitting (presented in SM S4) for the same Cu/Al ratios and Cu density for the same samples in Fig. 1 (Si/Al = 15) and seven other Cu_x zeolites (Si/Al = 4.5, 16, and 25; Table S4). Consistent with our observation, the site-isolated Cu²⁺ in CuO₂ in CuO₂ has a much larger fraction of Cu⁰ and Cu²⁺ ions during standard SCR catalyst, indicative of redox cycling between Cu²⁺ and Cu⁰ oxidation states coupled with the SCR catalytic cycle (22). The Cu²⁺ fraction in Table S4 is based on the Cu²⁺ on the isolated Cu²⁺ sites, which is the fraction of Cu²⁺ to convert one equivalent of NO and NH₃ per Cu²⁺, and to produce N₂ and H₂O (15, 16).

The inverse relationship between steady-state Cu²⁺ fraction and Cu/Al ratio (Fig. 2) is consistent with the behavior expected of a single-site catalyst, for which the active-site occupation state should depend only on the reaction

CO₂ → HCO₂H



structure of the ligand was confirmed by ³¹P NMR, ¹³C NMR, and ¹H NMR spectroscopy (Figures S1–S3, Supporting Information). The mesoporous silica support, SBA-15, was synthesized in a two-step procedure reported by N. P. Kovaleva et al.⁸ The resulting sample showed a type IV BET surface area of 950 m²/g and a Barrett-Joyner-Halenda (BJH) pore size of 6.2 nm (Table S1 and Figure S4, Supporting Information).

Ir-PNS/SA-15 (a) was synthesized by adding IrCl₃ onto SBA-15 to afford PNS/SA-15 (b) and this species underwent metathesis with ICl, hydride in refluxing anhydrous ethanol to afford Ir-PNS/SA-15 (b) (Figure 1, see the Supporting Information for a detailed procedure). For comparison, an intermediate product, the tethered Ir-supported Ru complex with a turnover frequency (TOF) of 1482 h⁻¹ for CO₂ hydrogenation to FA when PPh₃ was added under supercritical CO₂ conditions (80 °C, 18 MPa of total pressure).

The tethered Ru hybrid materials were characterized by a battery of techniques including FTIR, UV-vis, thermogravimetric analysis (TGA), N₂ physisorption, inductively coupled plasma optical emission (ICP-OES) and X-ray photoelectron spectroscopy (XPS) (see the Supporting Information). The FTIR spectra of unsupported PNP^t and Ir-PNP^t showed the Schiff base (=CH-NR= double-bond absorption at 1639 cm⁻¹, as well as p phenyl ring vibrations at 3067, 1587, 1435, 743, and 694 cm⁻¹. Similar peaks also appeared in the FTIR spectra of

CO₂ → 4NH₃ → 4N₂ + 4H₂O (1)

NO_x → N₂

literally with Cu density, as expected for a single-site catalyst. As shown here, however, experimental observations in the low-Cu density limit reveal a portion of the catalytic cycle in which O₂ activation by transient Cu²⁺ is coupled with Cu⁰ oxidation (Fig. 1A). These Cu²⁺ form from NH₃ solvated Cu ions with mobility restricted by electrostatic tethering to framework aluminum centers, a behavior that lies outside the canonical definition of a single-site catalyst (21).

We propose this phenomenon to assist for a molecularly detailed model to unify the seemingly disparate observations of the catalyst function of copper-exchanged chabazite (Cu_xCh) zeolites. In Cu_xCh, the primary active site for SCR is the standard selective catalytic reduction (SCR) of nitrogen oxides (NO_x, $x = 1, 2$) with ammonia (22). Supporting information for this article is available on the WWW under DOI: 10.1002/cctc.201200839.

Paolucci et al., *Science* **357**, 898–903 (2017)

1 September 2017

Downloaded from http://science.sciencemag.org/ on January 23, 2019

Important Energy-Related Catalysis

Complete oxidation



Applied Catalysis B: Environmental 39 (2002) 1–37



Complete oxidation of methane at low temperature over noble metal based catalysts: a review

Patrick Gelin*, Michel Prime

Laboratoire d'Application de la Chimie à l'Environnement, UMR CNRS 5634, Université Claude Bernard Lyon 1, Building Chevreul, 43 Boulevard du 11 Novembre 1918, 69622 Villeurbanne Cedex, France

Received 29 October 2001; received in revised form 20 March 2002; accepted 25 March 2002

Abstract

This review examines recent developments in the complete oxidation of methane at low temperature over noble metal based catalysts in patents and open literature. The abatement of natural gas vehicle (NGV) methane emissions is taken as an example of possible applications. The review develops current ideas about the properties of platinum and palladium supported on silica and alumina supports in the complete oxidation of methane under oxidising conditions, paying attention to reaction conditions. The influence of residual chloride ions on the catalytic activity, the kinetic aspects of the oxidation of methyl products on the active compounds are examined. The effect of sulphur containing and platinum supported catalysts which contain water and sulphur containing species on methane emissions is also discussed.

Keywords: Methane oxidation; Noble metals; Catalytic combustion; Low temperature; Lean burn NGV; Natural gas; Emission abatement; Platinum; Palladium; Catalyst poisoning; Water inhibition; Poisoning by sulphur and chlorine containing compounds; Kinetic studies; Silica; Alumina; Zirconia; Tin dioxide; Ceria; Ceria-zirconia solid solution; Zeolite; Aluminophosphate; Mixed oxide supports; Oxide additives; Bimetallic catalysts

1. Introduction

The catalytic combustion of methane has been extensively studied as an alternative to conventional thermal combustion and was reviewed [1–5]. This method was shown to be effective in producing energy in gas turbine combustors, while reducing emissions. Many studies were devoted to the design of catalytic

materials able to withstand high temperatures in atmospheres containing steam and oxygen. Another main application of catalytic total oxidation of hydrocarbons is the abatement of methane emissions from natural gas or methane combustion devices, being either catalytic or non-catalytic. This would in turn cover a wide range of applications, such as e.g. the abatement of methane emissions from lean-burn natural gas vehicles (NGVs).

Programs for the use of NGVs in urban areas, especially heavy-duty vehicles, are currently being developed very rapidly in most industrial countries.

* Corresponding author. Tel.: +33 4 72 43 11 48; fax: +33 4 72 44 81 14.
E-mail address: patrick.gelin@univ-lyon1.fr (P. Gelin).

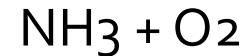
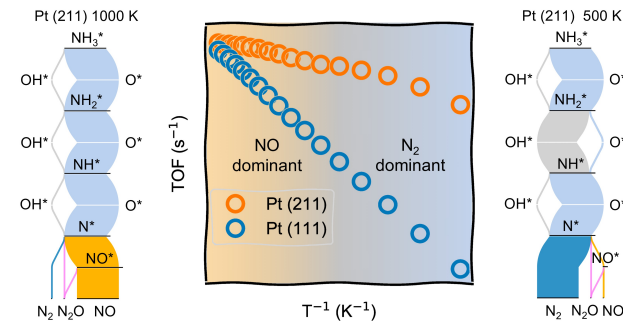
0926-3373/02/\$ – see front matter © 2002 Elsevier Science B.V. All rights reserved.
PII: S0926-3373(02)00076-0

Structure- and Temperature-Dependence of Pt-Catalyzed Ammonia Oxidation Rates and Selectivities

Hanyu Ma and William F. Schneider*

Department of Chemical and Biomolecular Engineering, University of Notre Dame, Notre Dame, Indiana 46556, United States

E-mail: wschneider@nd.edu



Important Energy-Related Catalysis

Dehydrogenation & Hydrogenation

Journal of Catalysis 345 (2017) 113–123

Contents lists available at ScienceDirect



Journal of Catalysis

journal homepage: www.elsevier.com/locate/jcat



Propane dehydrogenation catalyzed by gallosilicate MFI zeolites with perturbed acidity



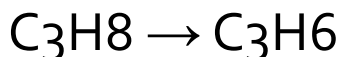
Seung-Won Cho^{a,1}, Wun-Gwi Kim^{a,1}, Jung-Seob So^a, Jason S. Moore^b, Yujun Liu^b, Ravindra S. Dixit^b, John G. Pendergast^b, Carsten Sievers^a, David S. Sholl^a, Sankar Nair^{a,*}, Christopher W. Jones^{a,*}

^aSchool of Chemical & Biomolecular Engineering, Georgia Institute of Technology, Atlanta, GA 30332-0100, United States

^bEngineering & Process Sciences, The Dow Chemical Company, Freeport, TX 77541, United States

ARTICLE INFO
Article history:
Received 28 March 2016
Revised 10 July 2016
Accepted 13 November 2016
Available online 8 December 2016

Keywords:
Propane
Dehydrogenation
Gallosilicate
Zeolite
Diss
3-Mercaptopropyl-n



1. Introduction

Propane dehydrogenation is one of the most important processes for the production of valuable polymers such as polypropylene and chemicals such as acrylonitrile and 2-propanol. The production of propane from catalytic dehydrogenation of propane (PDH) is carried out commercially by the Catofin process [1] and CBA Lummus [1–3]. The Catofin process uses a Pt-based catalyst. The CBA process uses a Cr-based catalyst in multiple parallel fixed bed reactors, while the Oleflex process uses a Pt-based catalyst in a fluidized bed reactor [14,15]. Both processes usually undergo rapid catalyst deactivation [16,17]. PDH processes have seen significant attention in recent years, especially in North America and the Middle East, due to abundant supplies of propane, and there are renewed efforts aimed at developing PDH catalysts and improving the stability, activity, and selectivity of these new catalysts. Propane feed stocks can be applied in propane aromatization. Propane aromatization catalysts have been widely used in the UOP/BP Cyclo dehydrocyclization process [18–22]. Ga-containing zeolites synthesized by

impregnation or ion-exchange into aluminosilicate H-ZSM-5 have been extensively studied [20–31]. Gallosilicate MFI can also be obtained by isomorphous substitution of Ga in the MFI zeolite framework [32,33], since Ga can be easily incorporated in the MFI framework.

In an early report, Bayse et al. reported that the specific synthesis method of the zeolite had a significant effect on the H-ZSM-5 did not have any effect on the propane conversion, but the addition of Ga increased the aromatic selectivity in all cases [24]. They also suggested that Ga-loaded H-ZSM-5 was better than the pure galliosilicate for propane aromatization. However, other studies have shown that Ga-loaded zeolites have higher propane aromatization selectivities than Ga ion-exchanged/impregnated H-ZSM-5 [14–36]. A reaction mechanism of propane aromatization using Ga loaded HZSM-5 was proposed by Gammerer et al. [37]. In this pathway, propane first protonates on the Brønsted acid sites. Then it undergoes either a dehydrogenation or a cracking step. A carbonium ion intermediate formed by the cracking step is then converted into propylene, followed by oligomerization and cyclization steps at the same site to form benzene.

The aromatic formation step is a PDH step when both Ga oxides species (Ga_2O_5) and Brønsted acid sites in the MFI pores are present. The strength of the Brønsted acid sites depends on the types of

REPORTS

rate of 10^{-3} $\text{M}_2 \cdot \text{year}^{-1}$ for this system is about 125. A value of 10^{-3} $\text{M}_2 \cdot \text{year}^{-1}$ would be required to bring SS-Cys₂ protonation rate in line with typical values for DCE dehydrogenation [38]. We find that the rate of jet power during the rise of $< 5 \times 10^{-3}$ $\text{M}_2 \cdot \text{year}^{-1}$ is $< 5 \times 10^{-3}$ $\text{M}_2 \cdot \text{year}^{-1}$ during the rise, we obtain a flux of < 0.7 mJ, in agreement with the literature [39]. This is consistent with the common disordered coupling in all accelerating objects from YSO to gamma ray bursts, suggested by Soker and Lasota [50].

As discussed above, the jet luminosity, as well as in the ratio of the radio emission to the X-ray emission, is proportional to the mass loss rate from a nonmagnetic DN. The detection of a jet in a DN with similar disordered coupling as that seen in the current work is consistent with the jet launching mechanism in CVn and XBhB. The radii of the jets in CVn and XBhB are much larger than those in young stellar objects (YSOs) and those of black holes, so WTA connect YSOs to CVn and XBhB via jets. The radius of the jet in XBhB, at accretion-powered jet

rate of < 0.7 mJ, is < 0.7 mJ, in agreement with the literature [39].

ACKNOWLEDGMENTS We thank F. Arribalzaga, J. G. Pendergast, and C. Sievers for useful discussions.

REFERENCES AND NOTES

1. D. Matto, C. D. Bailey, *Astronomy J.* **408**, 444 (2006).

2. D. Matto, T. Hines, T. Frail, *Rev. Mod. Phys.* **80**, 103 (2008).

3. D. Matto, T. Hines, T. Frail, *Rev. Mod. Phys.* **80**, 103 (2008).

4. D. Matto, *Science* **272**, 1164 (1996).

5. D. Matto, *Science* **272**, 1164 (1996).

6. A. O. Sano, T. Furukawa, A. Kojima, *Nature* **362**, 45 (1993).

7. A. O. Sano, T. Furukawa, A. Kojima, *Nature* **362**, 45 (1993).

8. A. O. Sano, T. Furukawa, A. Kojima, *Nature* **362**, 45 (1993).

9. A. O. Sano, T. Furukawa, A. Kojima, *Nature* **362**, 45 (1993).

10. A. O. Sano, T. Furukawa, A. Kojima, *Nature* **362**, 45 (1993).

11. A. O. Sano, T. Furukawa, A. Kojima, *Nature* **362**, 45 (1993).

12. A. O. Sano, T. Furukawa, A. Kojima, *Nature* **362**, 45 (1993).

13. A. O. Sano, T. Furukawa, A. Kojima, *Nature* **362**, 45 (1993).

14. R. F. Feeney, *J. Phys. Chem.* **63**, 2159 (1959).

15. R. F. Feeney, *J. Phys. Chem.* **63**, 2159 (1959).

16. R. F. Feeney, *J. Phys. Chem.* **63**, 2159 (1959).

17. R. F. Feeney, *J. Phys. Chem.* **63**, 2159 (1959).

18. R. F. Feeney, *J. Phys. Chem.* **63**, 2159 (1959).

19. R. F. Feeney, *J. Phys. Chem.* **63**, 2159 (1959).

20. R. F. Feeney, *J. Phys. Chem.* **63**, 2159 (1959).

21. R. F. Feeney, *J. Phys. Chem.* **63**, 2159 (1959).

22. R. F. Feeney, *J. Phys. Chem.* **63**, 2159 (1959).

23. R. F. Feeney, *J. Phys. Chem.* **63**, 2159 (1959).

24. R. F. Feeney, *J. Phys. Chem.* **63**, 2159 (1959).

25. R. F. Feeney, *J. Phys. Chem.* **63**, 2159 (1959).

26. R. F. Feeney, *J. Phys. Chem.* **63**, 2159 (1959).

27. R. F. Feeney, *J. Phys. Chem.* **63**, 2159 (1959).

28. R. F. Feeney, *J. Phys. Chem.* **63**, 2159 (1959).

29. R. F. Feeney, *J. Phys. Chem.* **63**, 2159 (1959).

30. R. F. Feeney, *J. Phys. Chem.* **63**, 2159 (1959).

31. R. F. Feeney, *J. Phys. Chem.* **63**, 2159 (1959).

32. R. F. Feeney, *J. Phys. Chem.* **63**, 2159 (1959).

33. R. F. Feeney, *J. Phys. Chem.* **63**, 2159 (1959).

34. R. F. Feeney, *J. Phys. Chem.* **63**, 2159 (1959).

35. R. F. Feeney, *J. Phys. Chem.* **63**, 2159 (1959).

36. R. F. Feeney, *J. Phys. Chem.* **63**, 2159 (1959).

37. A. O. Sano, T. Furukawa, A. Kojima, *Nature* **362**, 45 (1993).

38. A. O. Sano, T. Furukawa, A. Kojima, *Nature* **362**, 45 (1993).

39. A. O. Sano, T. Furukawa, A. Kojima, *Nature* **362**, 45 (1993).

40. A. O. Sano, T. Furukawa, A. Kojima, *Nature* **362**, 45 (1993).

41. D. Matto, *Science* **291**, 1375 (2001).

42. D. Matto, *Science* **291**, 1375 (2001).

43. D. Matto, *Science* **291**, 1375 (2001).

44. D. Matto, *Science* **291**, 1375 (2001).

45. D. Matto, *Science* **291**, 1375 (2001).

46. D. Matto, *Science* **291**, 1375 (2001).

47. D. Matto, *Science* **291**, 1375 (2001).

48. D. Matto, *Science* **291**, 1375 (2001).

49. D. Matto, *Science* **291**, 1375 (2001).

50. D. Matto, *Science* **291**, 1375 (2001).

51. D. Matto, *Science* **291**, 1375 (2001).

52. D. Matto, *Science* **291**, 1375 (2001).

53. D. Matto, *Science* **291**, 1375 (2001).

54. D. Matto, *Science* **291**, 1375 (2001).

55. D. Matto, *Science* **291**, 1375 (2001).

56. D. Matto, *Science* **291**, 1375 (2001).

57. D. Matto, *Science* **291**, 1375 (2001).

58. D. Matto, *Science* **291**, 1375 (2001).

59. D. Matto, *Science* **291**, 1375 (2001).

60. D. Matto, *Science* **291**, 1375 (2001).

61. D. Matto, *Science* **291**, 1375 (2001).

62. D. Matto, *Science* **291**, 1375 (2001).

63. D. Matto, *Science* **291**, 1375 (2001).

64. D. Matto, *Science* **291**, 1375 (2001).

65. D. Matto, *Science* **291**, 1375 (2001).

66. D. Matto, *Science* **291**, 1375 (2001).

67. D. Matto, *Science* **291**, 1375 (2001).

68. D. Matto, *Science* **291**, 1375 (2001).

69. D. Matto, *Science* **291**, 1375 (2001).

70. D. Matto, *Science* **291**, 1375 (2001).

71. D. Matto, *Science* **291**, 1375 (2001).

72. D. Matto, *Science* **291**, 1375 (2001).

73. D. Matto, *Science* **291**, 1375 (2001).

74. D. Matto, *Science* **291**, 1375 (2001).

75. D. Matto, *Science* **291**, 1375 (2001).

76. D. Matto, *Science* **291**, 1375 (2001).

77. D. Matto, *Science* **291**, 1375 (2001).

78. D. Matto, *Science* **291**, 1375 (2001).

79. D. Matto, *Science* **291**, 1375 (2001).

80. D. Matto, *Science* **291**, 1375 (2001).

81. D. Matto, *Science* **291**, 1375 (2001).

82. D. Matto, *Science* **291**, 1375 (2001).

83. D. Matto, *Science* **291**, 1375 (2001).

84. D. Matto, *Science* **291**, 1375 (2001).

85. D. Matto, *Science* **291**, 1375 (2001).

86. D. Matto, *Science* **291**, 1375 (2001).

87. D. Matto, *Science* **291**, 1375 (2001).

88. D. Matto, *Science* **291**, 1375 (2001).

89. D. Matto, *Science* **291**, 1375 (2001).

90. D. Matto, *Science* **291**, 1375 (2001).

91. D. Matto, *Science* **291**, 1375 (2001).

92. D. Matto, *Science* **291**, 1375 (2001).

93. D. Matto, *Science* **291**, 1375 (2001).

94. D. Matto, *Science* **291**, 1375 (2001).

95. D. Matto, *Science* **291**, 1375 (2001).

96. D. Matto, *Science* **291**, 1375 (2001).

97. D. Matto, *Science* **291**, 1375 (2001).

98. D. Matto, *Science* **291**, 1375 (2001).

99. D. Matto, *Science* **291**, 1375 (2001).

100. D. Matto, *Science* **291**, 1375 (2001).

101. D. Matto, *Science* **291**, 1375 (2001).

102. D. Matto, *Science* **291**, 1375 (2001).

103. D. Matto, *Science* **291**, 1375 (2001).

104. D. Matto, *Science* **291**, 1375 (2001).

105. D. Matto, *Science* **291**, 1375 (2001).

106. D. Matto, *Science* **291**, 1375 (2001).

107. D. Matto, *Science* **291**, 1375 (2001).

108. D. Matto, *Science* **291**, 1375 (2001).

109. D. Matto, *Science* **291**, 1375 (2001).

110. D. Matto, *Science* **291**, 1375 (2001).

111. D. Matto, *Science* **291**, 1375 (2001).

112. D. Matto, *Science* **291**, 1375 (2001).

113. D. Matto, *Science* **291**, 1375 (2001).

114. D. Matto, *Science* **291**, 1375 (2001).

115. D. Matto, *Science* **291**, 1375 (2001).

116. D. Matto, *Science* **291**, 1375 (2001).

117. D. Matto, *Science* **291**, 1375 (2001).

118. D. Matto, *Science* **291**, 1375 (2001).

119. D. Matto, *Science* **291**, 1375 (2001).

120. D. Matto, *Science* **291**, 1375 (2001).

121. D. Matto, *Science* **291**, 1375 (2001).

122. D. Matto, *Science* **291**, 1375 (2001).

123. D. Matto, *Science* **291**, 1375 (2001).

124. D. Matto, *Science* **291**, 1375 (2001).

125. D. Matto, *Science* **291**, 1375 (2001).

Important Energy-Related Catalysis



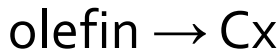
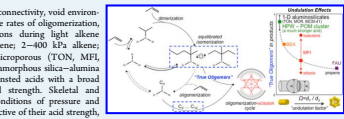
Effects of Void Environment and Acid Strength on Alkene Oligomerization Selectivity

Michele L. Sarazen,[†] Eric Doskočil,[‡] and Enrique Iglesia^{§,†}

[†]Department of Chemical and Biomolecular Engineering, University of California, Berkeley, Berkeley, California 94720, United States
[‡]BP Products North America Inc., 150 West Warrenville Rd, Naperville, Illinois 60563, United States

[§] Supporting Information

ABSTRACT: The effects of skeletal connecting, void environment, void size, and acid strength on the relative rates of oligomerization, β -scission, and isomerization reactions during light alkene conversion (ethylene, propene, isobutene; 2–400 kPa alkene; 473–533 K) were examined on microporous, MFI, SIAI, MOR, BEA, FAU, and mesoporous (amorphous silica-alumina (SIA)) MCM-41. Ketjen POM zeolite acted as a reference over a range of conditions of void size and acid strength. Skeletal and regiospecific equilibria under all conditions of pressure and conversion and on all catalysts, irrespective of their acid strength, void size, or framework connectivity, consistent with rapid hydride and proton shifts, alkylidene interconversions and also from intramolecular isotope scrambling in all oligomers formed from $^{2,3}\text{C}$ propene on TON, MFI, SIAI, and POM clusters. Previous claims of kinetic control of skeletal isomers in oligomerization catalysis through shape-selective effects conferred by void environments may have used inaccurate tabulated thermodynamics, as we show in the text.



KEYWORDS: oligomerization, β -scission, skeletal isomerization, zeolites, Brønsted acid catalyst

The oligomerization of alkenes on solid Brønsted acids provides an effective strategy to form new C–C bonds from small hydrocarbons.^{1–3} These processes become attractive as such small molecules are excluded from fuels, because of vapor pressure restrictions and as smaller molecules are available from biomass-derived hydrocarbons. Solid acids such as those derived from zeolites catalyze these reactions.⁴ Oligomerization occurs in parallel with its reverse reaction (β -scission in alkenes), albeit at

different C–C bond locations in the two directions; thermodynamic trends favor C–C bond formation over cleavage for smaller alkenes and at higher pressures and lower temperatures. Solid acids also catalyze concurrent hydrogen transfer and cyclization reactions, as well as skeletal and double-bond

Received: July 27, 2016
Revised: September 3, 2016
Published: September 21, 2016

DOI: 10.1021/acscatal.6b02128
ACSCatalysis 2016, 6, 7059–7070

Oligomerization



ARTICLE

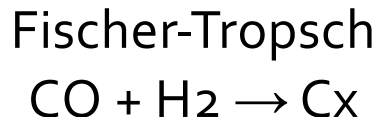
Received: 2 Jul 2014 | Accepted: 30 Jan 2015 | Published: 5 Mar 2015

DOI: 10.1038/ncomms7451

Metal organic framework-mediated synthesis of highly active and stable Fischer-Tropsch catalysts

Vera P. Santos^{1,2}, Tim A. Wezendonk¹, Juan José Delgado Jaén³, A. Iulian Dugulan⁴, Maxim A. Nasalevich¹, Husn-Ubayda Islam⁵, Adam Chojek², Sina Saripati¹, Xiaomin Sun¹, Abrar A. Hakeem⁶, Ard C.J. Koeken⁶, Matthijs Ruitenberg⁶, Thomas Davidian⁶, Garry R. Meima^{2,6}, Gopinathan Sankar⁶, Freek Kapteijn¹, Michiel Makkee¹ & Jorge Gascon¹

Depletion of crude oil resources and environmental concerns have driven a worldwide research on alternative processes for the production of commodity chemicals. Fischer-Tropsch synthesis is a process for flexible production of key chemicals from synthesis gas originating from non-petroleum-based sources. Although the use of iron-based catalysts would be preferred over the widely used cobalt, manufacturing methods that prevent their fast deactivation because of sintering, carbon deposition and phase changes have proven challenging. Here we present a strategy to produce highly dispersed iron carbides embedded in a matrix of porous carbon. Very high iron loadings (>40 wt %) are achieved while maintaining optimal dispersion of the active iron carbide phase when a metal organic framework is used as a catalyst precursor. The unique iron spatial confinement and the absence of large iron particles in the obtained solids minimize catalyst deactivation, resulting in high active and stable operation.



¹Catalysis Engineering, Department of Chemical Engineering, Delft University of Technology, Julianalaan 136, 2628 BL Delft, The Netherlands; ²Core R&D, Dow Benelux B.V., PO Box 48, 4530 AA Terneuzen, The Netherlands; ³Departamento de Ciencia de los Materiales e Ingeniería Metalúrgica y Química Inorgánica, Facultad de Ciencias, Universidad de Cádiz, Campus Rio San Pedro, 11510 Puerto Real, Cádiz, Spain; ⁴Fundamental Aspects of Materials and Processes, Institute of Chemical Sciences and Engineering, Politecnico di Milano, Via La Malfa 15/19, 20133 Milan, Italy; ⁵Department of Chemistry, University College London, 20 Gordon Street, WC1H 0AH London, UK; ⁶Hydrocarbons R&D, Dow Benelux B.V., PO Box 48, 4530 AA Terneuzen, The Netherlands. Correspondence and requests for materials should be addressed to J.G. (e-mail: j.gascon@tudelft.nl).

NATURE COMMUNICATIONS | 6:2451 | DOI: 10.1038/naturecommunications | www.nature.com/naturecommunications | © 2015 Macmillan Publishers Limited. All rights reserved.



Perspective
pubs.acs.org/acs катал

Mechanism of the Catalytic Conversion of Methanol to Hydrocarbons

Samia Ilias and Aditya Bhan*

Department of Chemical Engineering and Materials Science, University of Minnesota, Twin Cities, 421 Washington Avenue SE, Minneapolis, Minnesota 55455, United States

ABSTRACT: The discovery of the dual aromatic and olefin-based catalytic cycles in methanol-to-hydrocarbons (MTH) catalysts on acid zeolites has given a new context for relating structure–function relationships for more complex chemistries. This perspective explores six major steps involved in the hydrocarbon mechanism for MTH—olefin methylation, olefin cracking, hydrogen transfer, cyclization, aromatic methylation, and olefinic dealkylation—with a focus on what is known about them and mechanisms for their chemistries. The current mechanistic understanding of MTH limits structure–function relationships to the effect of the zeolite framework on the identity of the hydrocarbon pool and the resulting product selectivity. We emphasize the need for assessing the consequences of zeolite structure in MTH in terms of experimentally measured rates and activation barriers for individual reaction steps. In the absence of dual olefin and aromatic catalytic cycles to alter their relative propagation, we propose using ethene/isobutane selectivity as a measure to describe the relative rates of propagation for the aromatic- and olefin-based cycles.

KEYWORDS: methanol-to-hydrocarbons, methanol-to-olefins, hydrocarbon pool, zeolite, propane, methylation, cracking

1. INTRODUCTION

MTO

Global energy demand, steadily increasing from non-fossil fuel sources, supply the world with hydrocarbons (MTH) process over acac zeotite catalysts, first discovered by Mobil Research Laboratories in 1976,¹ has seen renewed interest in recent years for its ability to grow carbon chains from short-chain hydrocarbons. A syn-gas intermediate from such a natural gas^{2,3} and biomass^{4,5}. Methanol or its dehydration product dimethyl ether (DME) can be used as a feed to produce several different classes of hydrocarbons, including light olefins (methanol-to-olefins, MTO),^{6–9} gasoline-range hydrocarbons (methanol-to-gasoline, MTG),¹⁰ branched alkanes,^{10,11} and aromatics.¹² The selectivity to any of these classes of compounds is determined both by the zeolite topology and the operating conditions.

Since the discovery of MTH, there has been much debate regarding two aspects of the chemistry: (1) the origin of the first C–C bond location in the two directions; thermodynamic trends favor C–C bond formation over cleavage for smaller alkenes and at higher pressures and lower temperatures. Solid acids also catalyze concurrent hydrogen transfer and cyclization reactions, as well as skeletal and double-bond

that the catalyst induction period for MTH on H-ZSM-5 and H-SAPO-34 is highly sensitive to the impurity concentration in the methanol feed, indicating that if direct C–C coupling does occur, it operates at a rate significantly slower compared with the rate at which trace impurities initiate the reaction.¹⁰ Direct C–C coupling is often required for aromatic alkylation;

however, Matos et al. found that feeds of d_4 -DME over a D-SAPO-34 (in which 50% of the acid sites were H^+ and the other 50% were D^+) at 623 K resulted in an effluent containing approximately 25% d_4 -DME, 50% d_4 -DME, and 25% d_6 -DME. The bimodal distribution of D atoms in DME showed that H–D coupling is not the same as C–C coupling does not occur.¹⁷

Early work in MTH postulated a unisite mechanism on the basis of the observed catalytic induction period during which increasing the concentration of hydrocarbons greatly increased the rate of conversion of DME to DMSO and branched alkanes.^{10,11} The selectivity to any of these classes of compounds is determined both by the zeolite topology and the operating conditions.

Since the discovery of MTH, there has been much debate

regarding two aspects of the chemistry: (1) the origin of the first C–C bond and (2) the mechanism by which MTH proceeds. In the past decade, a broad consensus has emerged on the importance of coordination of the zeolites to couple directly at rates relevant for state-of-the-art MTH catalysts.¹³ Lestzoghe and co-workers^{14,15} used ONIOM methods to calculate activation energies and rate constants for multiple pathways to form C–C bonds starting from two methanol molecules and the activation energies and rates for direct C–C coupling to be surprisingly high (~200 kJ mol^{−1}). Experiments using fractionally distilled methanol demonstrated

the reaction of methanol alone over H-ZSM-5 at 512 K. Additionally, Lestzoghe et al.¹⁶ reported that by combining DMSO with higher alcohols, the rate readily decreases to near zero under reaction conditions on H-ZSM-5; the kinetic induction period could be substantially reduced, indicating the important catalytic role of olefins in MTH. Dessau and LaPierre^{10,11} outlined a reaction mechanism for MTH based on

Received: October 6, 2012
Revised: November 25, 2012
Published: December 5, 2012

DOI: 10.1021/acscatal.2c00683 | ACS Catal. 2013, 3, 18–31

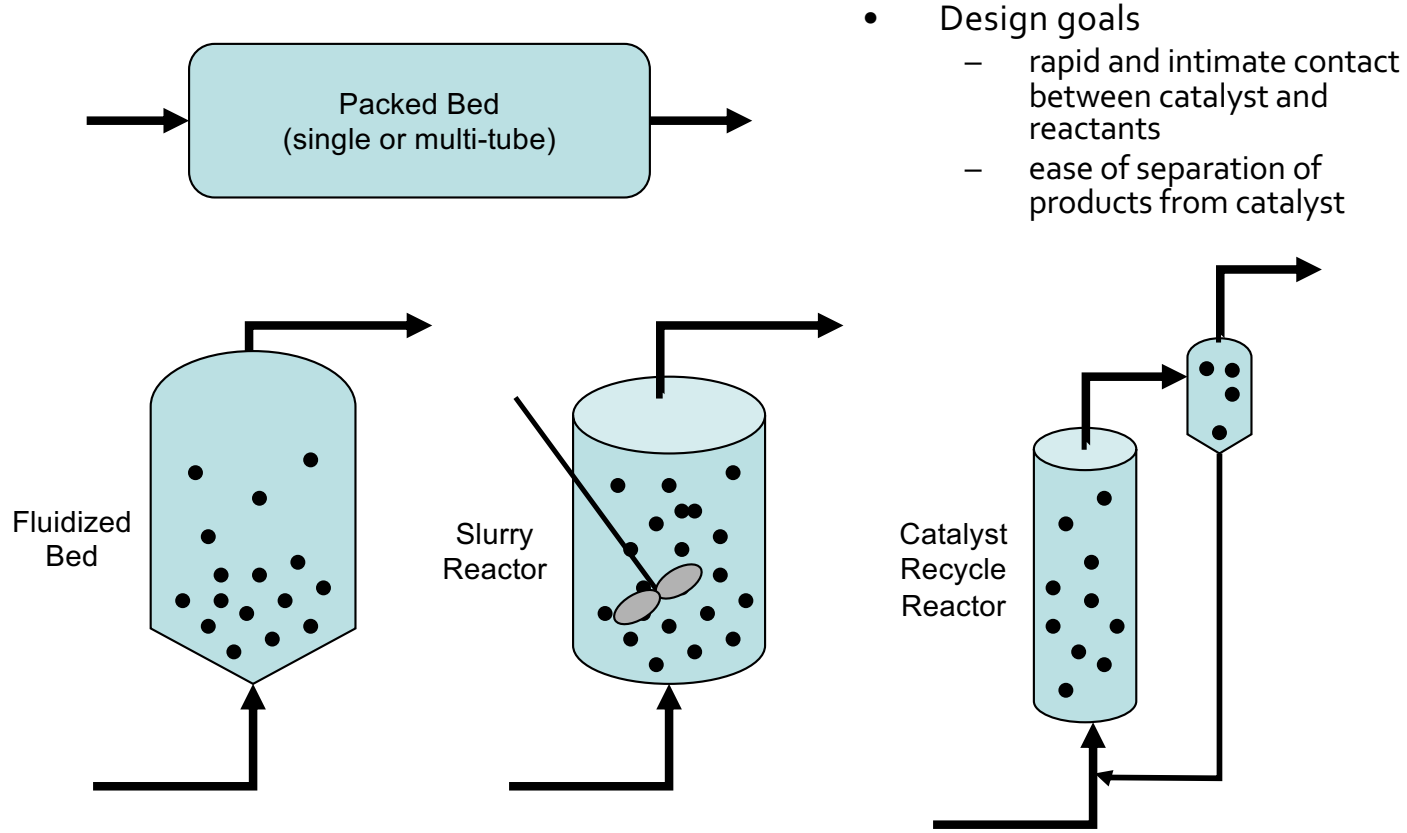


W.F. Schneider

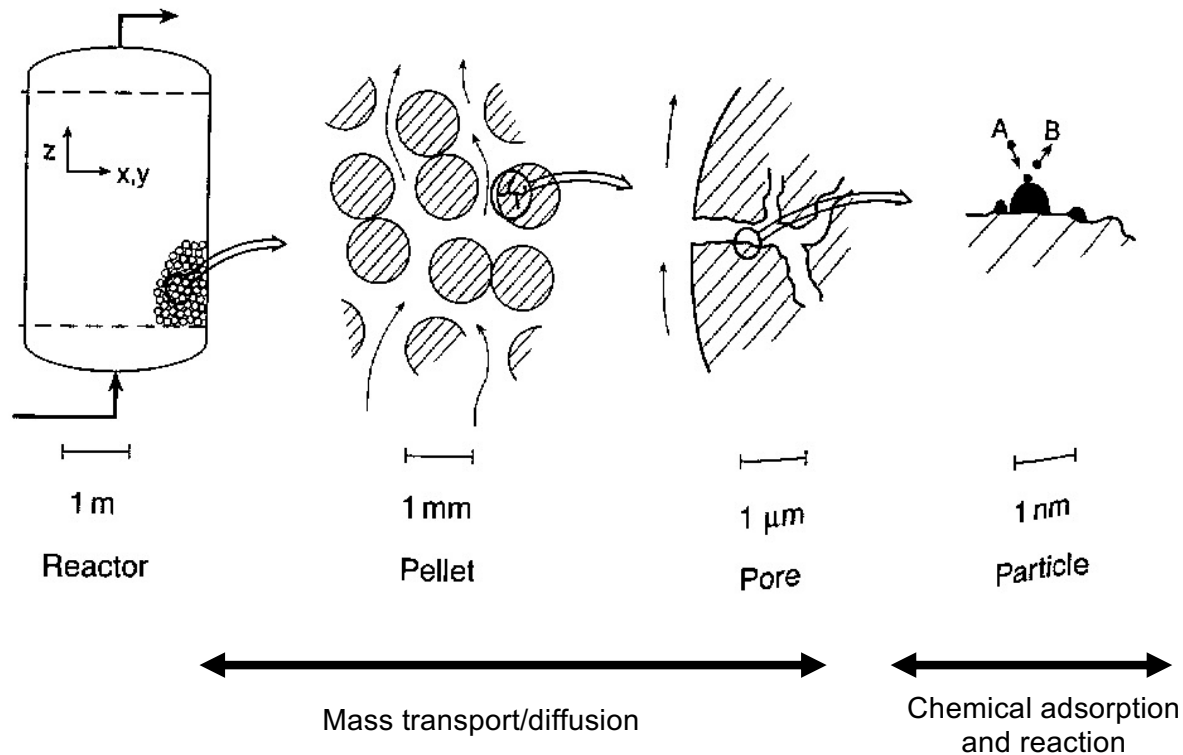
CBE 60546 - Heterogeneous Catalysis

18

Heterogeneous Catalytic Reactors

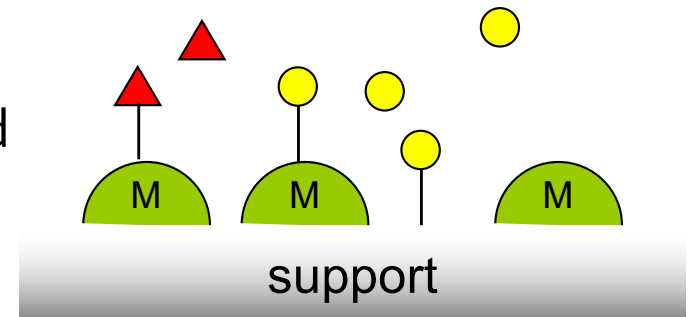


Length Scales in Heterogeneous Catalysis



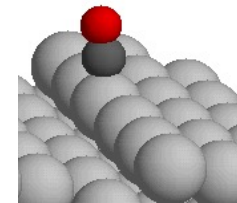
Characteristics of Heterogeneous Supported Catalysts

- Surface area:
 - Amount of internal support surface accessible to a fluid
 - Measured by gas adsorption isotherms
- Loading:
 - Mass of transition metal per mass of support
- Dispersion:
 - Percent of metal atoms accessible to a fluid



Rates of Catalytic Reactions

- Pseudo-homogeneous reaction rate
 - $r = \text{moles} / \text{volume} \cdot \text{time}$
- Mass-based rate
 - $r' = \text{moles} / \text{mass}_{\text{cat}} \cdot \text{time}$
 - $r' = r / \rho_{\text{cat}}$
- *Heterogeneous reactions happen at surfaces*
- Area-based rate
 - $r'' = \text{moles} / \text{area}_{\text{cat}} \cdot \text{time}$
 - $r'' = r' / SA, \quad SA = \text{area} / \text{mass}$
- *Heterogeneous reactions happen at active sites*
- Active site-based rate
 - Turn-over frequency $TOF = \text{moles} / \text{site} \cdot \text{time}$
 - $TOF = r'' / \rho_{\text{site}}$



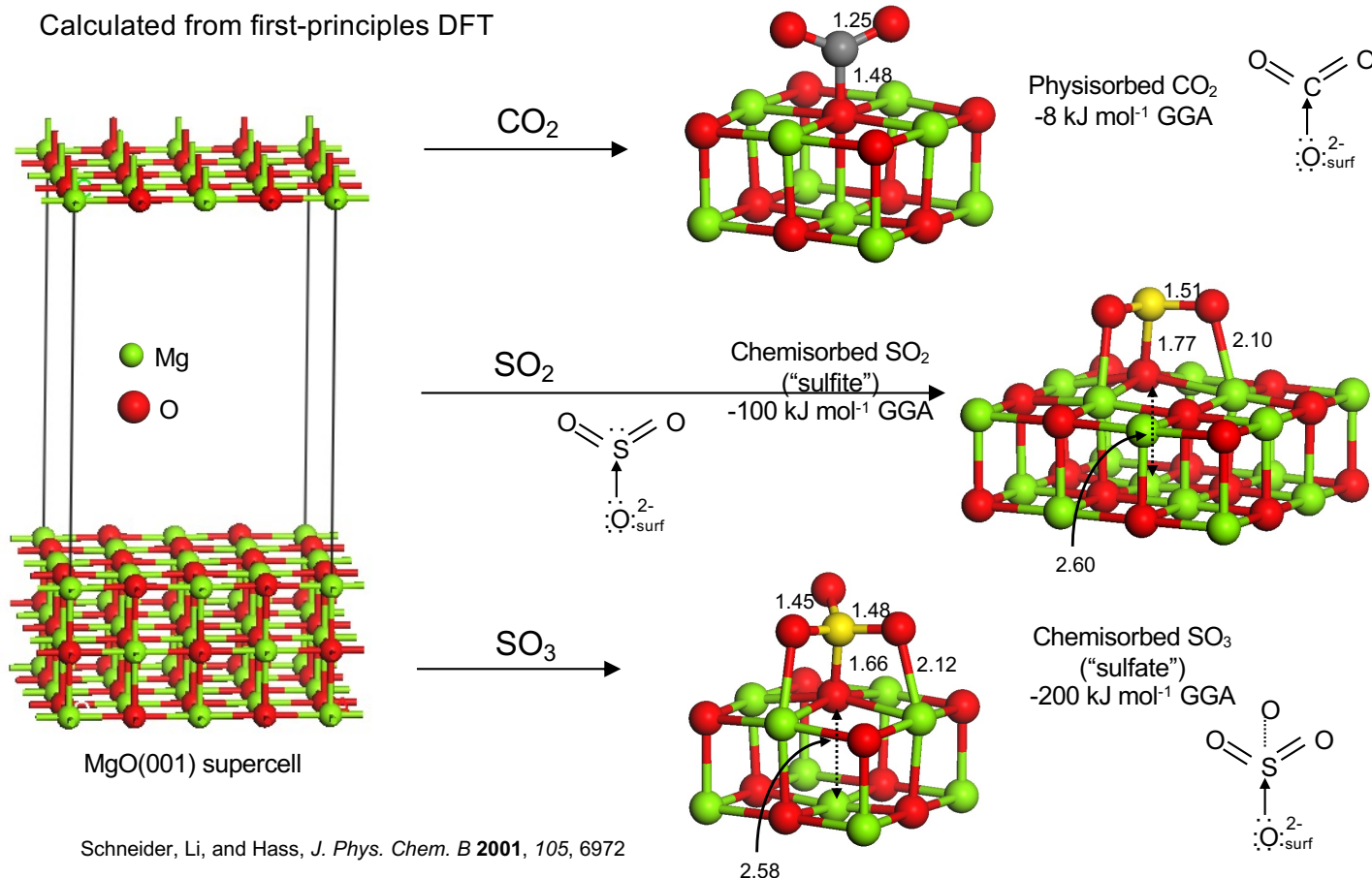
$TOF (s^{-1})$
Hetero. cats. $\sim 10^1$
Enzymes $\sim 10^6$

Adsorption and Reaction at Solid Surfaces

- Physisorption: weak van der Waals attraction of a fluid (like N₂ gas) for any surface
 - $E_{ads} \sim 10 - 40 \text{ kJ/mol}$
 - Low temperature phenomenon
 - Exploited in measuring gross surface area
- Chemisorption: chemical bond formation between a fluid molecule (like CO or ethylene) and a surface site
 - $E_{ads} \sim 100 - 500 \text{ kJ/mol}$
 - Essential element of catalytic activity
 - Exploited in measuring catalytically active sites



Comparing Physi- and Chemisorption on MgO(001)



Concentrations in Heterogeneous Reactions Kinetics

- Fluid concentrations

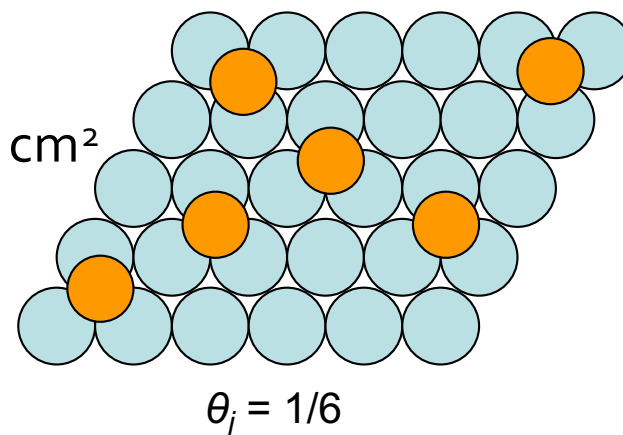
- Traditionally reported as pressures (torr, atm, bar)
- Ideal gas assumption: $P_j = C_j RT$

- Surface concentrations

- “Coverage” per unit area
 - $n_j = \text{moles}_j / \text{area}$
- Maximum coverage called monolayer
 - 1 ML: $n_{j,\max} = \sim 10^{15} \text{ molecules / cm}^2$
- Fractional coverage
 - $\vartheta_j = n_j / n_{j,\max}$
 - $0 \leq \vartheta_j \leq 1$

$$\text{Rate} = f(P_j, \vartheta_j)$$

Metal particle surface



Adsorption Isotherms

- Molecules in gas and surface are in dynamic equilibrium
$$A \text{ (g)} + M \text{ (surface)} \leftrightarrow M\text{-}A$$
- Isotherm describes pressure dependence of equilibrium
- Langmuir isotherm proposed by Irving Langmuir, GE, 1915
 - (1932 Nobel Prize)
 - Adsorption saturates at 1 monolayer
 - All sites are equivalent
 - Adsorption is independent of coverage

$$\text{rate}_a = k_a P_A N \theta^*$$

$$\text{rate}_d = k_d N \theta_A$$

$$\frac{\text{Site conservation}}{\theta_A + \theta^* = 1}$$

$$+ \quad \frac{\text{Equilibrium}}{\text{rate}_{\text{ads}} = \text{rate}_{\text{des}}} \longrightarrow$$

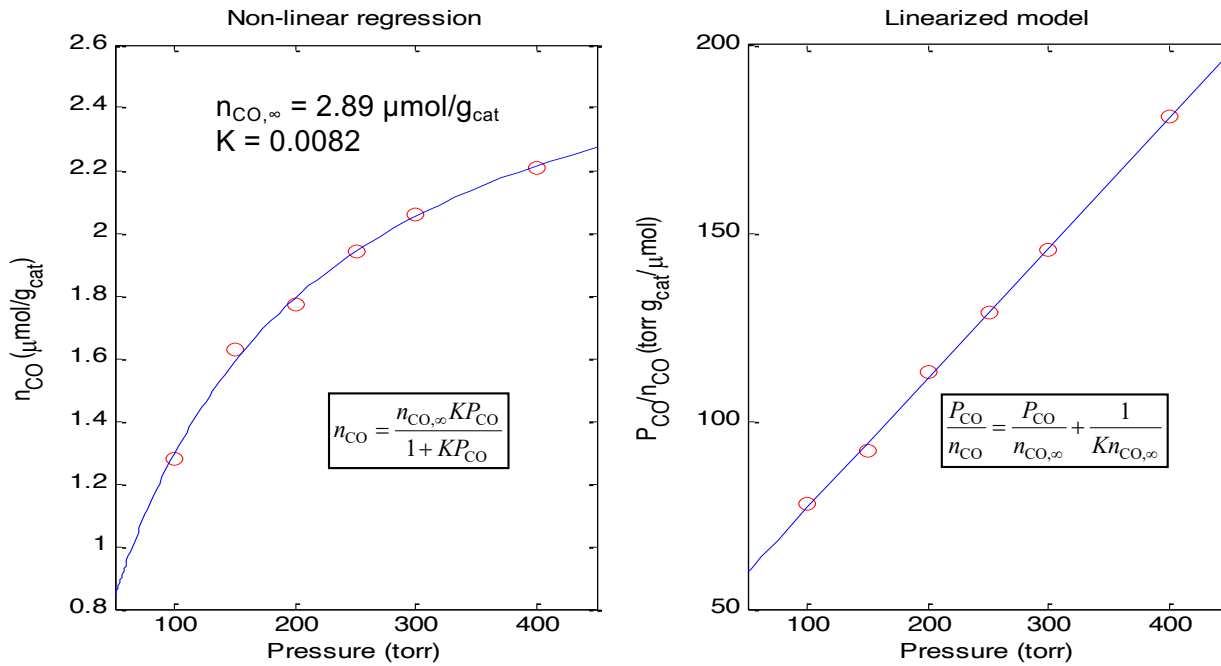
$$\theta_A = \frac{KP_A}{1 + KP_A}, \quad K = k_a/k_d$$



Using the Langmuir Isotherm

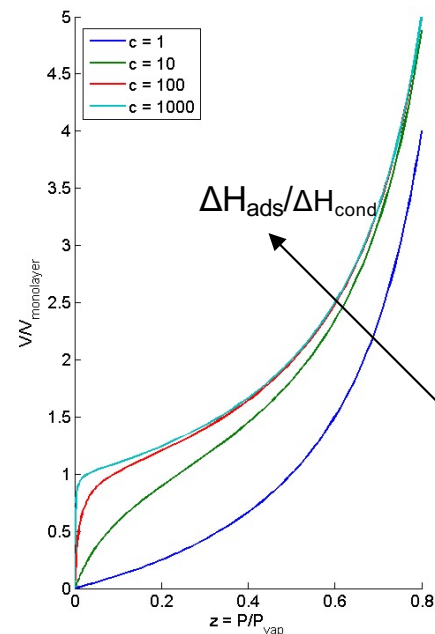
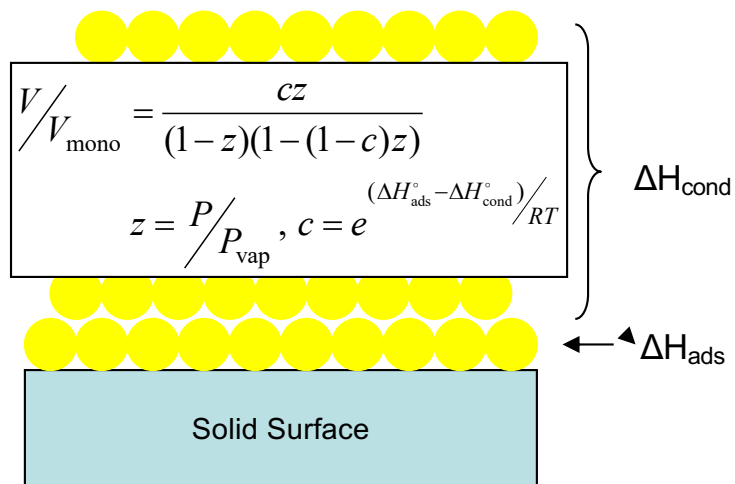
- Example: CO adsorption on 10% Ru/Al₂O₃ @ 100°C

P_{CO} (torr)	100	150	200	250	300	400
$n_{CO_{ads}}$ ($\mu\text{mol/g}_{\text{cat}}$)	1.28	1.63	1.77	1.94	2.06	2.21

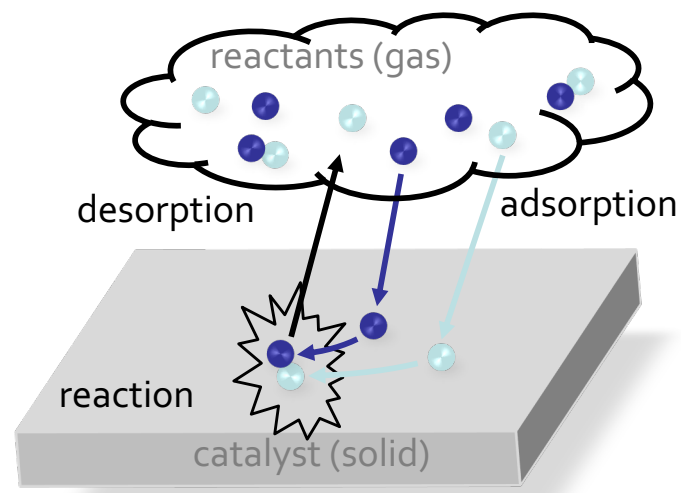


Brunauer-Emmett-Teller Isotherm (BET)

- Relaxes Langmuir restriction to single layer adsorption
 - Monolayer adsorption; multilayer condensation
- Useful for total surface area measurement
 - Adsorption of boiling N₂ (78 K)



Chemical Processes in Heterogeneous Catalysis



Temperature Programmed Desorption

$$r_{\text{des}} = -\frac{d\theta}{dt} = \tilde{\nu}(\theta)\theta^n \exp\left(\frac{-E_{\text{des}}^\ddagger(\theta)}{k_B T}\right)$$

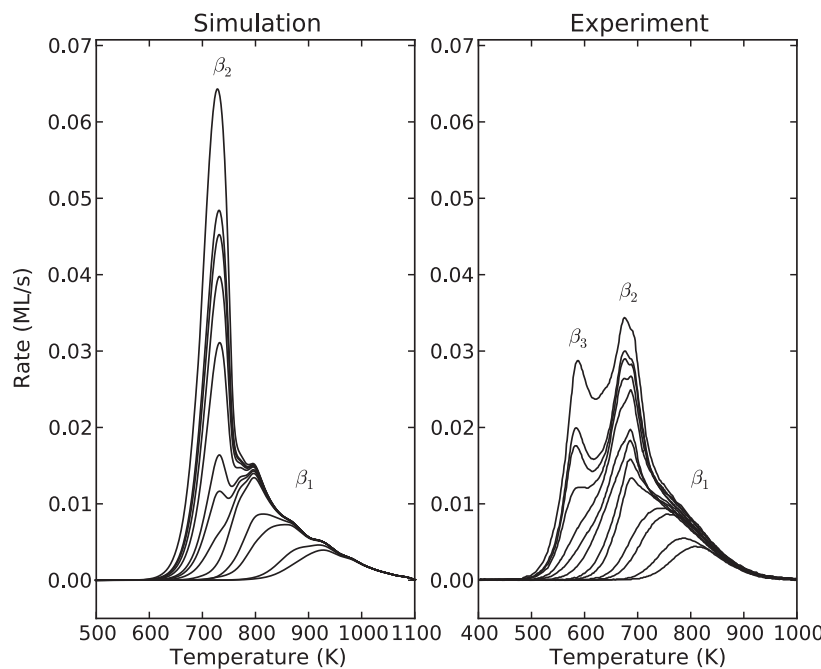
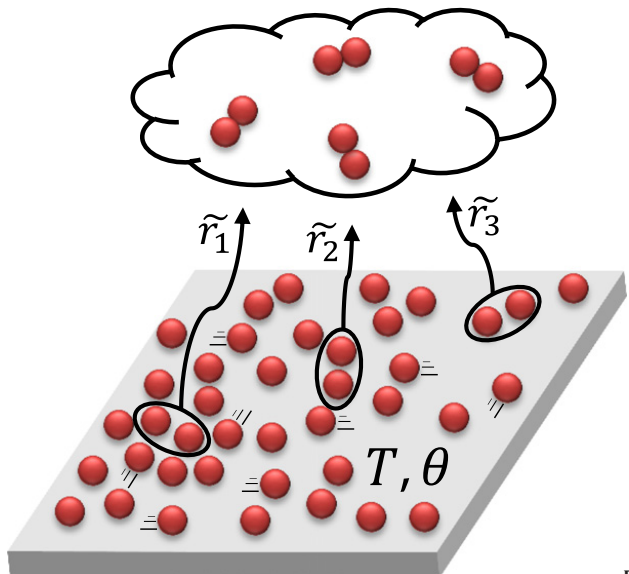


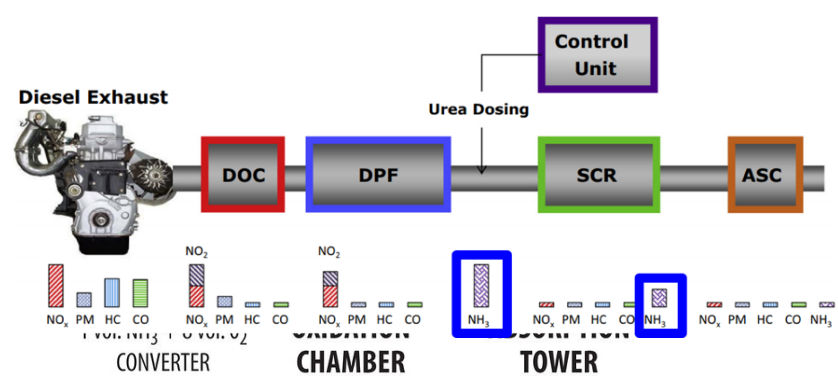
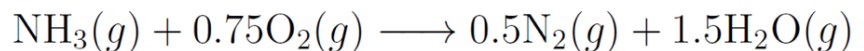
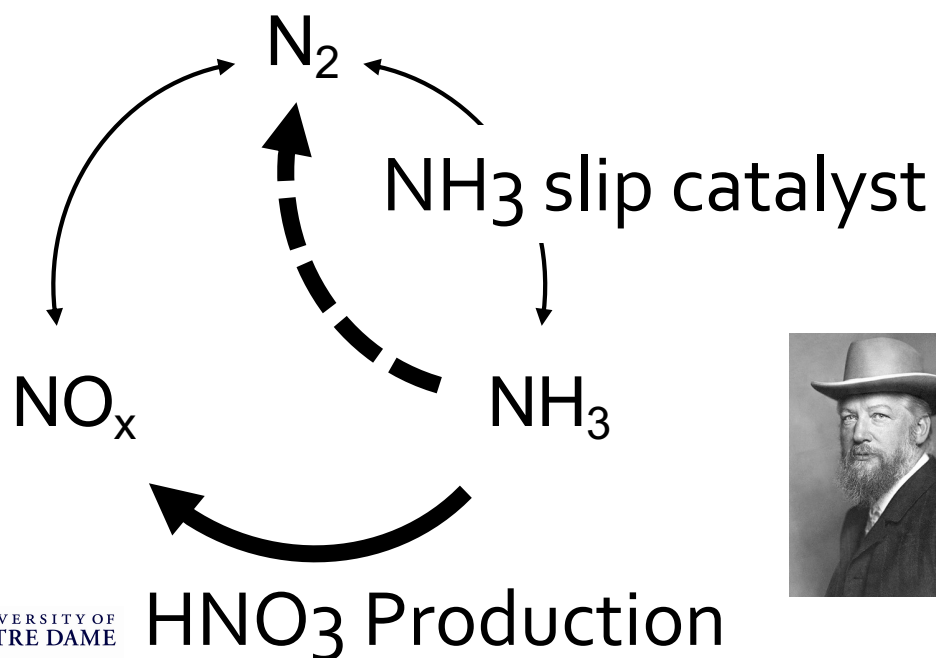
Fig. 3. Simulated (left) and renormalized experimental TPD results (right) for Pt(111)-O from Ref. [10]. Heating rate is 8 K s^{-1} and initial coverages are 0.073, 0.093, 0.164, 0.194, 0.258, 0.291, 0.331, 0.363, 0.467, 0.534, 0.579, 0.606, and 0.75 ML.

Langmuir-Hinshelwood Kinetics



Nitrogen Chemistry

- Nitrogen transformations intimately connected with human kind's use of energy, production of food, and protection of the environment

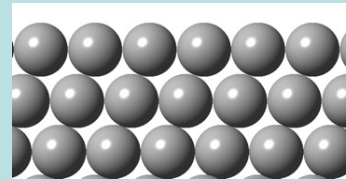


Friedrich Wilhelm Ostwald
1908 Nobel Prize

Catalyst Surface Structure

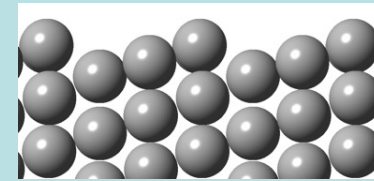
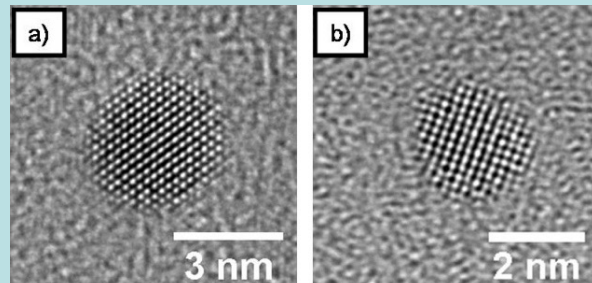
Ostwald process

Pt Gauze



NH₃ slip

Pt Nanoparticles



Microkinetic Modeling

Reaction Mechanism

- (1) $O_2(g) + 2^* \longleftrightarrow 2O^*$
- (2) $NH_3(g) + * \longleftrightarrow NH_3^*$
- (3) $NH_3^* + O^* \longleftrightarrow NH_2^* + OH^*$
- (4) $NH_2^* + O^* \longleftrightarrow NH^* + OH^*$
- (5) $NH^* + O^* \longleftrightarrow N^* + OH^*$
- (6) $NH_3^* + OH^* \longleftrightarrow NH_2^* + H_2O^*$
- (7) $NH_2^* + OH^* \longleftrightarrow NH^* + H_2O^*$
- (8) $NH^* + OH^* \longleftrightarrow N^* + H_2O^*$
- (9) $OH^* + OH^* \longleftrightarrow O^* + H_2O^*$
- (10) $H_2O^* \longleftrightarrow H_2O(g) + *$
- (11) $N^* + N^* \longleftrightarrow N_2(g) + 2^*$
- (12) $N^* + O^* \longleftrightarrow NO^* + *$
- (13) $NO^* \longleftrightarrow NO(g) + *$
- (14) $N^* + NO^* \longleftrightarrow N_2O^*$
- (15) $N_2O^* \longleftrightarrow N_2O(g) + *$

Transition State Theory

Surface reactions

$$k_f(T) = \frac{k_B T}{h} \frac{q^\ddagger}{q_{\text{react}}} \exp\left(-\frac{E_a}{k_B T}\right)$$

$$r_{AB} = k_{AB} \theta_A \theta_B$$

Non-activated adsorption

$$k_{\text{ads}} = \frac{A}{\sqrt{2\pi m k_B T}}$$

$$r_A = k_{\text{ads}} P_A$$

Thermodynamic Consistency

$$k_r(T) = K_{\text{eq}}(T)/k_f(T)$$

μkinetic model

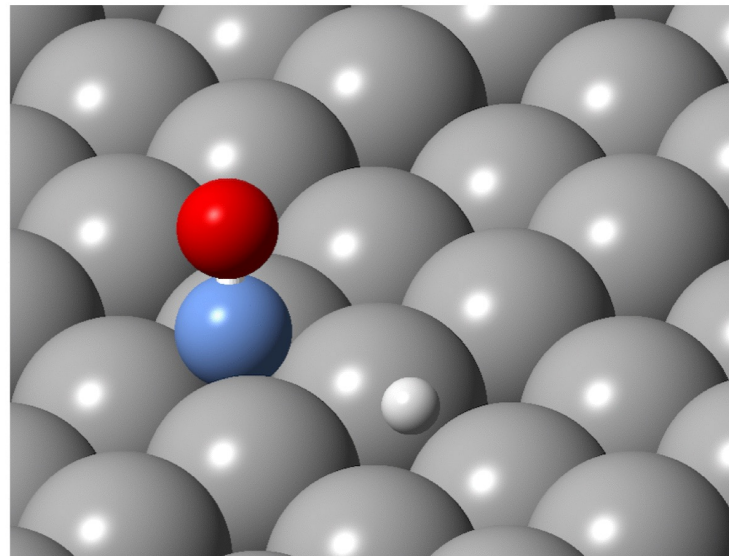
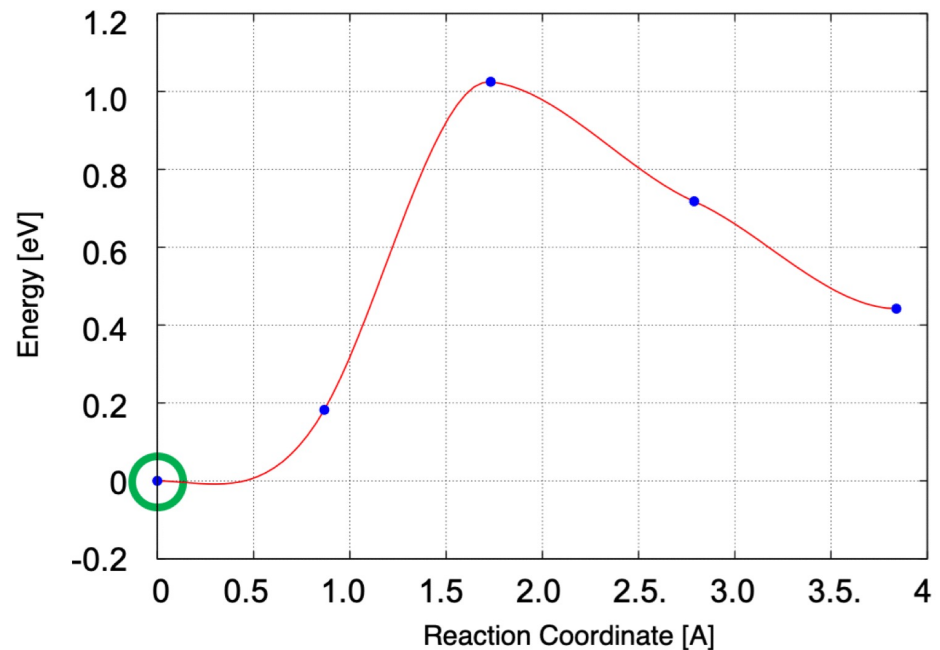
$P_{NH_3}, P_{O_2}, P_{H_2O}, T$

Mass + site balances

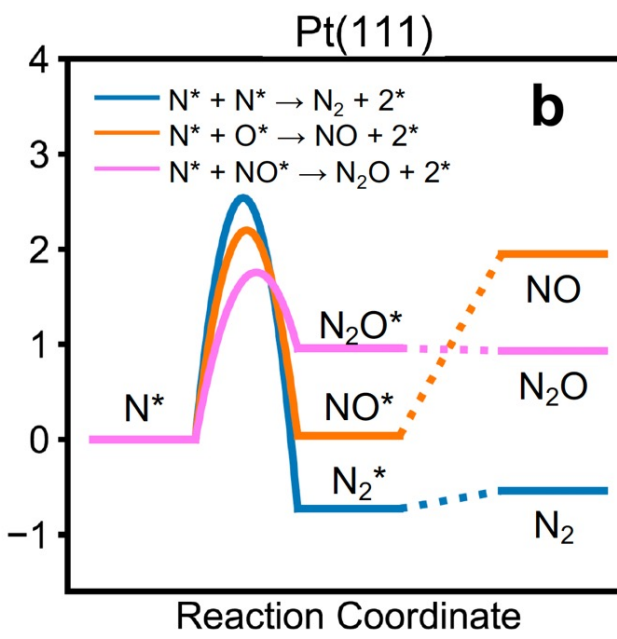
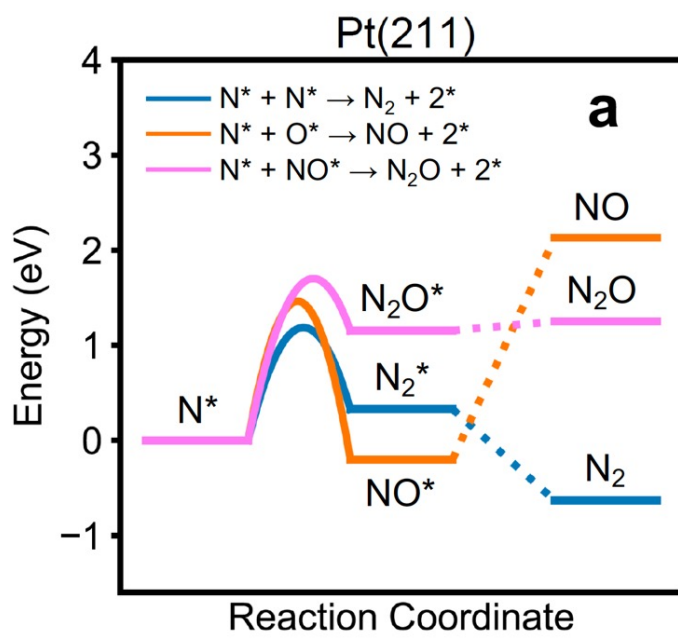
Coverages
Rates

DFT Reaction Pathways

Supercell/PAW/GGA Vasp computations for intermediates, pathways, activation energies and prefactors of relevant surface reactions.

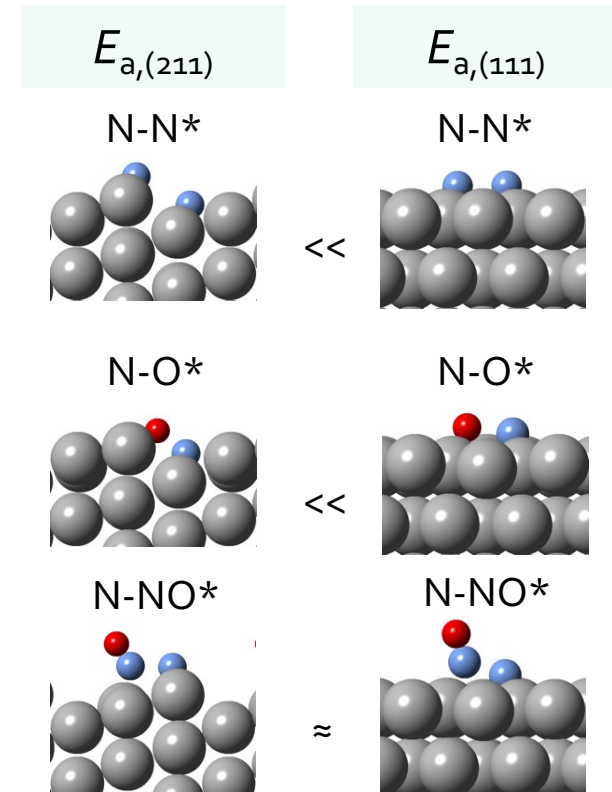


Recombination Pathways

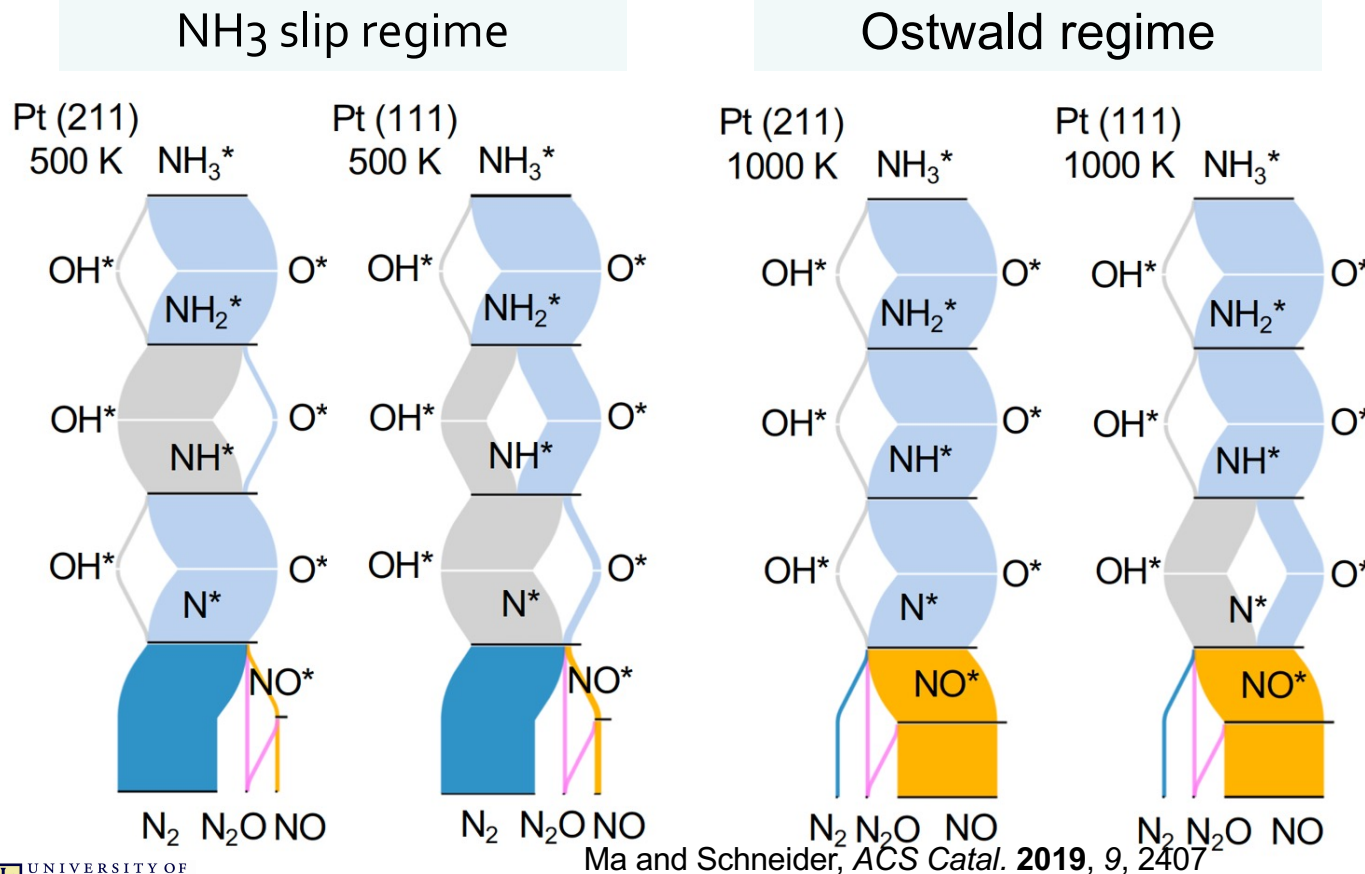


Non-BEP behavior, structure sensitive

Ma and Schneider, ACS Catal. 2019, 9, 2407

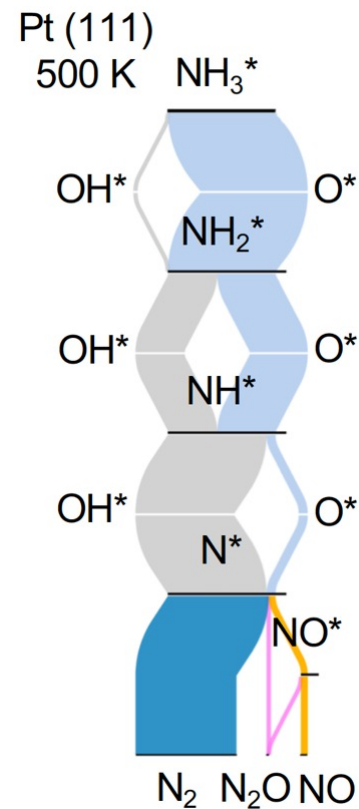
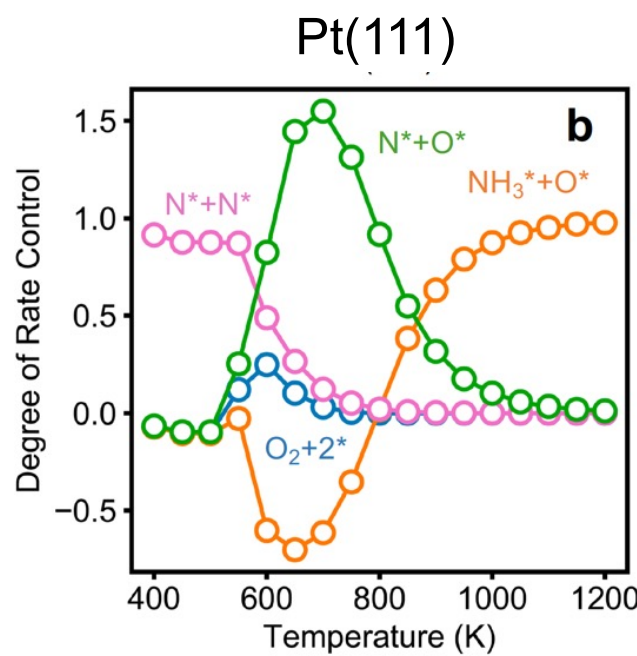
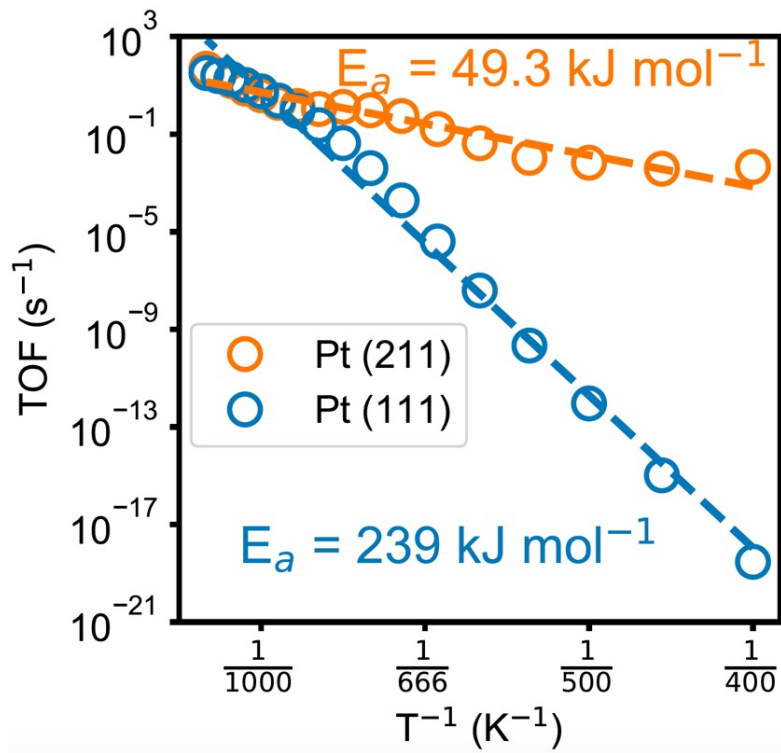


Net Reaction Fluxes



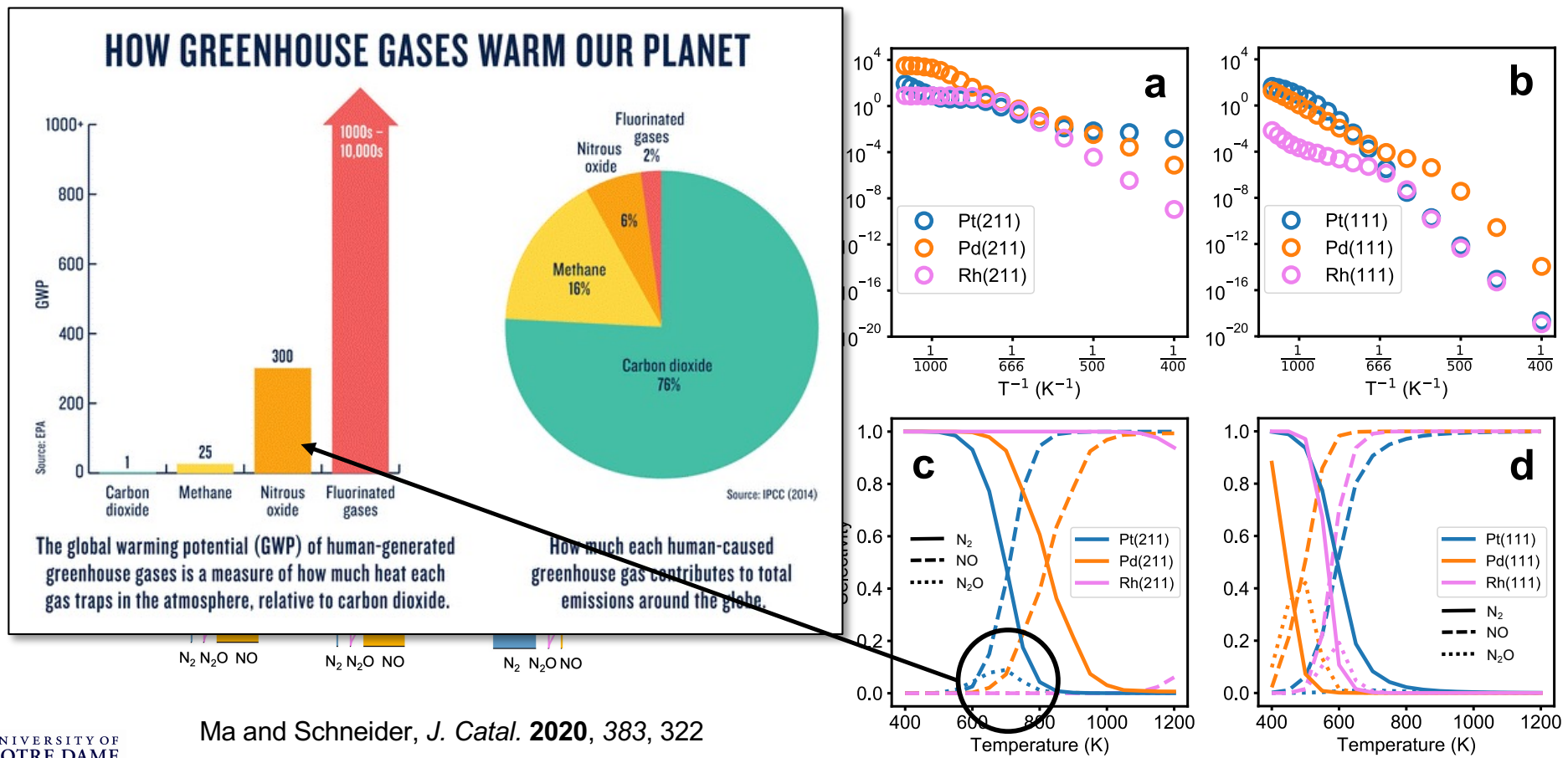
- Preferred pathways sensitive to facet...
- ...and to temperature
- But products are not!

Does Structure Matter?

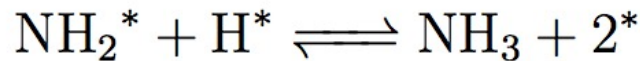
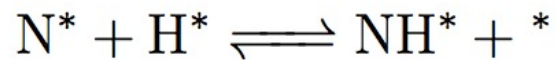
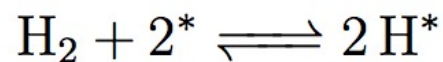
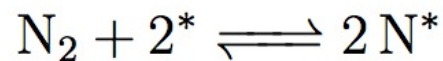


Ma and Schneider, ACS Catal. 2019, 9, 2407

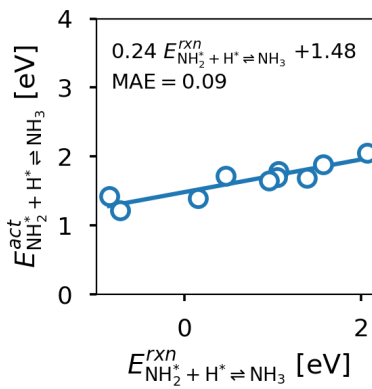
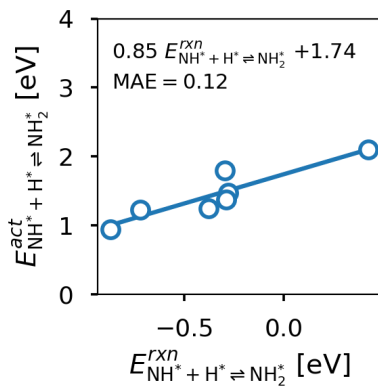
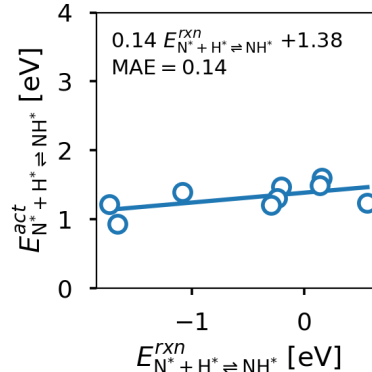
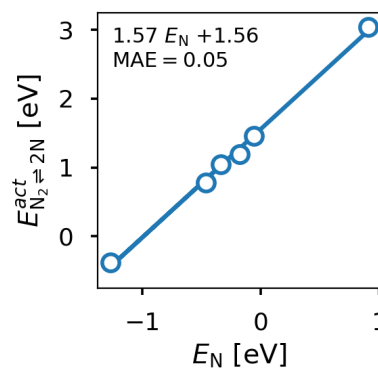
Does Metal Catalyst Matter?



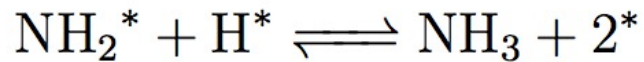
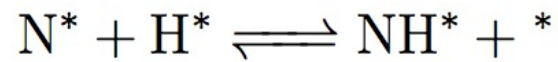
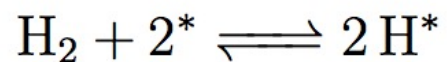
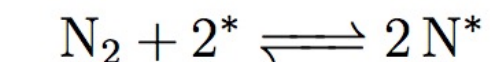
Brønsted-Evans-Polyani Relationships



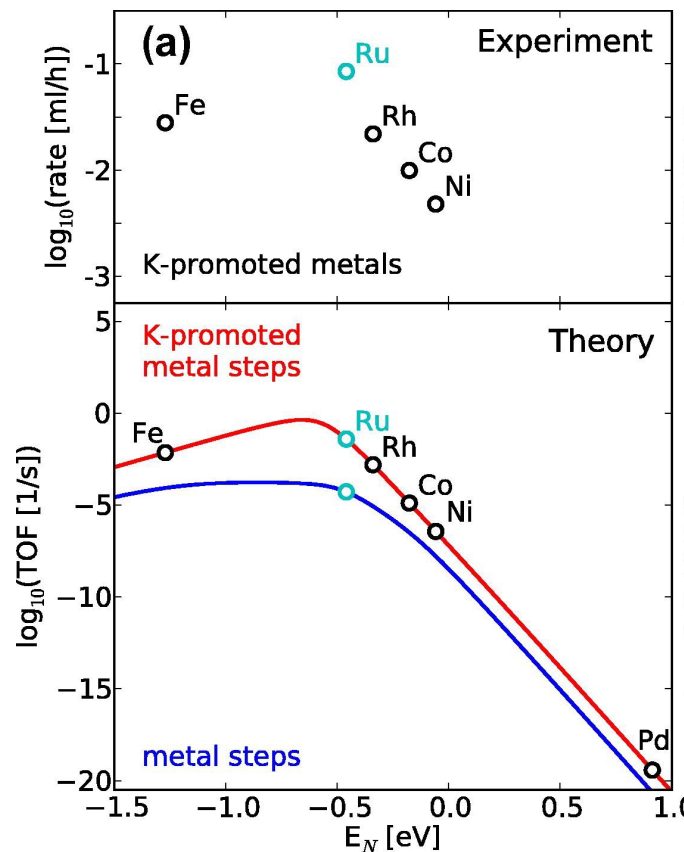
Intrinsic correlations between reaction energies and barriers limit achievable rates



Sabatier Plot



Intrinsic correlations between reaction energies and barriers limit achievable rates



Vojvodic *et al.* *Chem. Phys. Lett.* 2014, 598, 108